

IFIC/00-28  
FTUV/00-0605  
HD-THEP-00-7  
FZJ-IKP(TH)-00-14

# S-wave $K\pi$ scattering in chiral perturbation theory with resonances

Matthias Jamin<sup>1</sup>, José Antonio Oller<sup>2</sup> and Antonio Pich<sup>3</sup>

<sup>1</sup> *Institut für Theoretische Physik, Universität Heidelberg,  
Philosophenweg 16, D-69120 Heidelberg, Germany*

<sup>2</sup> *Forschungszentrum Jülich, Institut für Kernphysik (Theorie),  
D-52425 Jülich, Germany*

<sup>3</sup> *Departament de Física Teòrica - IFIC, Universitat de València - CSIC,  
Apt. Correus 2085, E-46071 València, Spain*

**Abstract:** We present a detailed analysis of S-wave  $K\pi$  scattering up to 2 GeV, making use of the resonance chiral Lagrangian predictions together with a suitable unitarisation method. Our approach incorporates known theoretical constraints at low and high energies. The present experimental status, with partly conflicting data from different experiments, is discussed. Our analysis allows to resolve some experimental ambiguities, but better data are needed in order to determine the cross-section in the higher-energy range. Our best fits are used to determine the masses and widths of the relevant scalar resonances in this energy region.

PACS: 11.80.Et, 12.39.Fe, 13.75.Lb, 13.85.Fb

Keywords: Partial-wave analysis, Chiral Lagrangians, Meson-meson interactions,  
Inelastic scattering: two-particle final states

# 1 Introduction

Chiral Perturbation Theory ( $\chi$ PT) [1–7] provides a very powerful framework to study the low-energy dynamics of the lightest pseudoscalar octet. The QCD chiral symmetry constraints imply the pseudo-Goldstone nature of the  $\pi$ ,  $K$  and  $\eta$  mesons and determine their interactions at very low energies.

To describe the resonance region around 1 GeV, additional non-trivial dynamical information is needed. One can construct a chiral-symmetric Effective Field Theory with resonance fields as explicit degrees of freedom [8, 9]. Although not as predictive as the standard chiral Lagrangian for the pseudo-Goldstone mesons, the resonance chiral Lagrangian [8] turns out to provide interesting results, once some short-distance dynamical QCD constraints are taken into account [9]. At tree level, this Lagrangian encodes the large- $N_c$  properties of QCD [10, 11], in the approximation of keeping only the dominant lowest-mass resonance multiplets [12].

The  $\chi$ PT loops incorporate the unitarity field theory constraints in a perturbative way, order by order in the momentum expansion. In the resonance region, the low-energy expansion breaks down and some kind of resummation of those chiral loops is required to satisfy unitarity [13–21]. This effect appears to be crucial for a correct understanding of the scalar sector, because the S-wave rescattering of two pseudoscalars is very strong.

In this paper, we present an attempt to describe S-wave  $K\pi$  scattering up to 2 GeV, making use of the resonance chiral Lagrangian predictions together with a suitable unitarisation method. The analysis is far from trivial, owing to the very unsatisfactory experimental status of the scalar sector, with partly conflicting data from different experiments. Even the masses and widths of the dominant scalar resonances are not clearly established, since the large unitarity corrections tend to mask the resonance behaviour.

A good understanding of the scalar isospin-1/2 system is required in order to improve the determination of the strange quark mass from QCD sum rules for the strangeness-changing scalar current [22–27], since the phenomenological parametrisation of the corresponding spectral function can be related to the  $K\pi$  scalar form factor. We plan to discuss this form factor in detail in a subsequent publication [28].

In section 2 we collect the one-loop  $\chi$ PT results for the  $K\pi$  scattering amplitude, including scalar and vector resonance contributions. Our unitarisation approach for the elastic channel is discussed in section 3. Section 4 analyses the experimental data up to 1.3 GeV and several  $\chi$ PT-inspired fits are performed. At higher energies, one needs to include inelastic channels; the dominant two-body  $K\pi \rightarrow K\eta, K\eta'$  modes are incorporated in section 5, and used in section 6 to fit the higher-energy data up to 2 GeV. Our fits

determine the resonance poles of the  $T$  matrix in the complex plane; this is worked out in section 7, where we compare results for the resonance masses and widths from different fits. Our conclusions are briefly summarised in section 8. To simplify the presentation, we refer to refs. [4–9] for details on the chiral formalism and notations, while some technical aspects and cumbersome formulae are relegated into appendices.

## 2 Chiral expansion for the $K\pi$ scattering amplitudes

Up to one loop in the chiral expansion the  $K\pi$  scattering amplitudes have been calculated by Bernard, Kaiser and Meißner [29] and resonance contributions have been included by the same authors in [30]. We shall just review the main expressions for the  $K\pi$  amplitudes to make our work selfcontained.

Since the pion and the kaon have isospin 1 and 1/2 respectively, there exist two independent  $K\pi$  amplitudes  $T_{K\pi}^{1/2}$  and  $T_{K\pi}^{3/2}$  (in the following, for simplicity, we shall drop the subscript “ $K\pi$ ”). The charge-two process  $K^+\pi^+ \rightarrow K^+\pi^+$  is purely  $I = 3/2$  whereas the process  $K^+\pi^- \rightarrow K^+\pi^-$  contains both  $I = 1/2$  and  $I = 3/2$  components. Both amplitudes depend on the Mandelstam variables  $s$ ,  $t$  and  $u$  and are related by  $s \leftrightarrow u$  crossing. From this relation one finds<sup>1</sup>

$$T^{1/2}(s, t, u) = \frac{3}{2} T^{3/2}(u, t, s) - \frac{1}{2} T^{3/2}(s, t, u). \quad (2.1)$$

Therefore it is sufficient to give here only the  $I = 3/2$  amplitude  $T^{3/2}$ .

At order  $p^4$  in the  $\chi$ PT expansion including resonances,  $T^{3/2}$  can be decomposed as follows

$$T^{3/2} = T^{(2)} + T_R^{(4)} + T_U^{(4)} + T_T^{(4)}, \quad (2.2)$$

where  $T^{(2)}$  is the leading order  $p^2$  contribution already known from current algebra [32].  $T_R^{(4)}$ ,  $T_U^{(4)}$  and  $T_T^{(4)}$  are order  $p^4$  resonance, unitarity and tadpole corrections respectively. We have assumed that at the resonance-mass scale the low-energy constants  $L_i$  in the order  $p^4$  chiral Lagrangian are saturated by resonance exchange [8,9]. The tree-level contribution  $T^{(2)}$  is given by

$$T^{(2)}(s) = \frac{1}{2f_K f_\pi} (M_K^2 + M_\pi^2 - s). \quad (2.3)$$

In writing eq. (2.3), we have absorbed some order  $p^4$  corrections into  $T^{(2)}$  by replacing  $1/f_\pi^2$  with  $1/(f_K f_\pi)$ .

---

<sup>1</sup>For further details the reader is referred to refs. [29,31].

Below, we list explicit expressions for the order  $p^4$  contributions  $T_R^{(4)}$ ,  $T_U^{(4)}$  and  $T_T^{(4)}$  to the amplitude  $T^{3/2}$  in  $\chi$ PT with resonances. The resonance contribution  $T_R^{(4)}(s, t, u)$  is given by

$$\begin{aligned}
T_R^{(4)} = & \frac{1}{f_K^2 f_\pi^2} \left\{ \frac{G_V^2}{2} \left[ \frac{t(u-s)}{M_\rho^2 - t} + \frac{u(t-s) + \Delta_{K\pi}^2}{M_{K^*}^2 - u} \right] \right. \\
& + \frac{1}{M_{K_0^*}^2 - u} [c_d u - (c_d - c_m) \Sigma_{K\pi}]^2 - \frac{c_m^2}{M_S^2} \Delta_{K\pi}^2 \\
& \left. + \frac{1}{3} \left[ \frac{4}{M_{S_1}^2 - t} - \frac{1}{M_S^2 - t} \right] [c_d t - 2(c_d - c_m) M_K^2] [c_d t - 2(c_d - c_m) M_\pi^2] \right\}, \quad (2.4)
\end{aligned}$$

where we defined the constants  $\Delta_{K\pi} \equiv (M_K^2 - M_\pi^2)$  and  $\Sigma_{K\pi} \equiv (M_K^2 + M_\pi^2)$ .  $G_V$  as well as  $c_d$  and  $c_m$  are coupling constants of the vector and scalar mesons in the chiral resonance Lagrangian of refs. [8,9] respectively. For the coupling constants of the scalar singlet meson  $S_1$ ,  $\tilde{c}_d$  and  $\tilde{c}_m$ , we have already used the large- $N_c$  constraints  $\tilde{c}_d = c_d/\sqrt{3}$  and  $\tilde{c}_m = c_m/\sqrt{3}$ .  $M_S$  refers to the mass of a generic scalar octet meson and we shall always employ the large- $N_c$  result  $M_{S_1} = M_S$ .

The unitarity correction  $T_U^{(4)}(s, t, u)$  has originally been calculated in ref. [29] and takes the form

$$\begin{aligned}
T_U^{(4)} = & \frac{1}{4f_K^2 f_\pi^2} \left\{ t(u-s) [2M_{\pi\pi}^r(t) + M_{KK}^r(t)] + \frac{3}{2} \left\{ (s-t) [L_{\pi K}(u) + L_{K\eta_8}(u)] \right. \right. \\
& - u (M_{\pi K}^r(u) + M_{K\eta_8}^r(u)) \left. \right\} + \Delta_{K\pi}^2 (M_{\pi K}^r(u) + M_{K\eta_8}^r(u)) \left. \right\} \\
& + \frac{1}{2} \Delta_{K\pi} [(5u - 2\Sigma_{K\pi}) K_{\pi K}(u) + (3u - 2\Sigma_{K\pi}) K_{K\eta_8}(u)] + (s - \Sigma_{K\pi})^2 J_{\pi K}^r(s) \\
& + \frac{1}{8} [11u^2 - 12\Sigma_{K\pi} u + 4\Sigma_{K\pi}^2] J_{\pi K}^r(u) + \frac{3}{8} \left( u - \frac{2}{3}\Sigma_{K\pi} \right)^2 J_{K\eta_8}^r(u) \\
& + \frac{1}{2} t(2t - M_\pi^2) J_{\pi\pi}^r(t) + \frac{3}{4} t^2 J_{KK}^r(t) + \frac{1}{2} M_\pi^2 \left( t - \frac{8}{9} M_K^2 \right) J_{\eta_8\eta_8}^r(t) \left. \right\}. \quad (2.5)
\end{aligned}$$

We have already corrected for two misprints which appeared in the original publication [29] and the explicit form of the loop functions can be found in appendix A. The unitarity correction has also recently been checked independently in ref. [33].

Finally, the tadpole contribution  $T_T^{(4)}$  reads

$$T_T^{(4)} = - \frac{\Delta_{K\pi}}{16f_K f_\pi} [3\mu_\pi - 2\mu_K - \mu_{\eta_8}], \quad (2.6)$$

with  $\mu_P$  being functions which depend on the renormalisation scale  $\mu$  and are given by

$$\mu_P = \frac{M_P^2}{32\pi^2 f_\pi^2} \ln \left( \frac{M_P^2}{\mu^2} \right). \quad (2.7)$$

It has been assumed that the resonance contribution saturates the low-energy constants  $L_i$  and thus, in accordance with ref. [8], in the following we always set the renormalisation scale  $\mu = M_\rho$ , where this saturation is found to take place. Both, the resonance as well as the tadpole contribution above, take different forms compared to the original papers [29, 30], because we chose to write the tree-level term (2.3) differently. However, we have independently calculated these terms finding agreement with [30].

Since in this work we are only interested in the S-wave  $K\pi$  scattering amplitude, the partial wave projection still has to be performed. Generally, the partial wave amplitudes  $t_l^I(s)$  are given by

$$t_l^I(s) = \frac{1}{32\pi} \int_{-1}^1 dz P_l(z) T_{K\pi}^I(s, z), \quad (2.8)$$

where  $l$  is the total angular momentum,  $z = \cos \theta$  is the scattering angle in the c.m. system and  $P_l(z)$  are Legendre polynomials [34].

### 3 Unitarisation of the amplitudes

A numerical inspection of eq. (2.2) shows that already at energies of the order of 1 GeV the unitarity correction  $T_V^{(4)}$  is rather large. Since we aim at describing S-wave  $K\pi$  scattering well above 1 GeV, we have to resort to methods which unitarise the partial wave amplitudes. The approach we are going to use is based on the N/D method [35] and has been developed in refs. [20, 21, 36]. It can be derived by working out the partial wave amplitudes from a perturbative loop expansion in terms of the unphysical cuts. The generated partial waves are then matched with the ones derived from next-to-leading order  $\chi$ PT [3] including in addition the explicit exchange of resonances [8].

Restricting oneself to two-body unitarity and neglecting the unphysical cut contributions, with the help of the N/D method [35] in ref. [20] the corresponding general structure of a partial wave amplitude was derived. This structure was shown to match with the local tree-level  $\chi$ PT amplitudes plus the  $s$ -channel exchange of explicit resonance fields. It was also estimated that the contributions of the unphysical cuts in the physical region below 1 GeV for the  $I = 1/2$  meson-meson S-waves amount just to a few percent. Then, in ref. [21, 36] the generalisation of this approach to include the unphysical cuts up to one loop in  $\chi$ PT was established. Note that the present expansion, treating the unphysical cut contributions as small quantities, can be implemented as a chiral loop expansion of these contributions. This means that at the tree level our amplitudes are crossing symmetric, e.g. resonance exchanges are included in all the  $s$ ,  $t$  and  $u$ -channels, and that the resulting

partial waves amplitudes fulfil the N/D equations exactly in the right hand cut and up to one loop in  $\chi$ PT for the unphysical cuts. This is precisely the order required to match with the chiral expressions of ref. [30], where the local and pole terms [3, 8] were supplied with loops calculated at  $\mathcal{O}(p^4)$  in  $\chi$ PT. In refs. [36, 37] the method described above has already been used to study the strongly interacting Higgs sector and elastic  $\pi N$  scattering, respectively.

Up to the considered order, we can write the unitarised partial wave amplitude  $\tilde{t}_l^I(s)$  as [21]:<sup>2</sup>

$$\tilde{t}_l^I(s) = \frac{N_l^I(s)}{\left(1 - g_{K\pi}^I(s) N_l^I(s)\right)}, \quad (3.1)$$

with

$$N_l^I(s) = t_l^I(s) - g_{K\pi}^I(s) \left(t_l^{I(2)}(s)\right)^2, \quad (3.2)$$

and

$$g_{K\pi}^I(s) = 16\pi \bar{J}_{K\pi}(s) + c_{K\pi}^I. \quad (3.3)$$

On the right-hand side of eq. (3.2),  $t_l^{I(2)}(s)$  refers to the leading  $\mathcal{O}(p^2)$  expression of  $t_l^I(s)$ , with  $t_l^I(s)$  itself being calculated at the one-loop level in  $\chi$ PT plus resonances.  $\bar{J}(s)$  is the standard two-particle one-loop integral as given in appendix A, and the  $c_{K\pi}^I$  are arbitrary constants, not fixed by the unitarisation procedure, which have to be real in order to satisfy unitarity. Reexpanding (3.1) up to one loop, also taking into account eq. (3.2), one can immediately match the resulting expression to the chiral amplitudes collected in section 2.

It is easy to see that eq. (3.1) satisfies elastic unitarity above the  $K\pi$  threshold and below the inelastic ones, namely:

$$\text{Im} \tilde{t}_l^I(s) = \sigma_{K\pi}(s) |\tilde{t}_l^I(s)|^2, \quad (3.4)$$

since by construction  $\text{Im} N_l^I(s) = 0$  in the  $K\pi$  physical region and

$$\text{Im} g_{K\pi}^I(s + i0) = \sigma_{K\pi}(s) \equiv \sqrt{(1 - s_+/s)(1 - s_-/s)}, \quad (3.5)$$

for  $s \geq s_+$  where  $s_+ = (M_K + M_\pi)^2$  and  $s_- = (M_K - M_\pi)^2$ .

As long as we only consider a single channel,  $\tilde{t}_l^I(s)$  and  $N_l^I(s)$  are scalar functions. In ref. [21] the rather straightforward generalisation of eq. (3.1) to coupled channels where  $\tilde{t}_l^I(s)$  and  $N_l^I(s)$  become matrices is also given and we shall come back to it in section 5 below.

---

<sup>2</sup>For more details, we refer the reader to section 3.2 of the review [21].

## 4 Fitting the elastic channel

Experimentally, it has been observed that the  $I = 1/2$   $K\pi$  scattering amplitude turns out to be elastic below roughly 1.3 GeV and the same was found for the  $I = 3/2$  amplitude up to 1.9 GeV. Therefore, in this energy range we should be able to describe the experimental data on  $K\pi$  scattering with the unitarised chiral expressions presented in the previous two sections. First we shall comment on the experimental data which we included in our fits, before we explain the actual fitting procedure and our results.

The two most recent experiments on  $K\pi$  scattering have been performed by Estabrooks et al. [38] and Aston et al. [39, 40]. Estabrooks et al. measured charged  $K\pi$  scattering for all four charge combinations and were thus able to separate the  $I = 1/2$  and  $I = 3/2$  components in the elastic region below 1.3 GeV. Aston et al. only considered  $K^-\pi^+$  scattering. In this case the S-wave amplitude in terms of phase shifts and inelasticities is given as follows:

$$A_0 = a_0 e^{i\phi_0} = A_0^{1/2} + \frac{1}{2} A_0^{3/2} = \frac{1}{2i} \left( \eta_0^{1/2} e^{2i\delta_0^{1/2}} - 1 \right) + \frac{1}{4i} \left( \eta_0^{3/2} e^{2i\delta_0^{3/2}} - 1 \right), \quad (4.1)$$

where  $\eta_0^I$  and  $\delta_0^I$  are the inelasticities and phase shifts for the  $I = 1/2$  and  $I = 3/2$  channel respectively. In writing eq. (4.1) we have adopted the normalisation of refs. [38–40] for  $A_0$ . In ref. [38],  $\delta_0^{1/2}$  has been extracted for  $\sqrt{s} = 0.73 - 1.30$  GeV, and  $\delta_0^{3/2}$  for  $0.73 - 1.72$  GeV. In this work it was also demonstrated that below 1.3 GeV, the scattering is purely elastic, that is,  $\eta_0^{1/2} = \eta_0^{3/2} = 1$ , whereas it was found that  $\eta_0^{3/2} = 1$  in the full energy range. On the other hand in ref. [40] only  $a_0$  and  $\phi_0$  up to  $\sqrt{s} = 2.52$  GeV were given.

Because the  $I = 3/2$  component of the scattering amplitude was only measured directly by Estabrooks et al. [38], we have decided to also include older data for  $\delta_0^{3/2}$  in our fits [41–44]. The last three experiments only presented data for the  $K^-\pi^-$  cross section and one still has to extract  $\delta_0^{3/2}$  from the given cross sections. In addition, rather different energy intervals have been used by the experimental groups [38, 41–44] for calculating cross sections and phase shifts. To be able to combine the data consistently, we thus also included an error in the energy. Nevertheless, it turned out that the combined  $\chi^2/d.o.f.$  for our fits was only of the order of one if we increased the error in all the experiments [38, 41–44] by a factor of two. The increase of errors for these data is implied in the rest of our work.

In terms of the unitarised chiral expressions, the isospin amplitudes  $A_0^I$  are given by

$$A_0^I(s) = \frac{\sigma_{K\pi}(s) N_0^I(s)}{(1 - g_{K\pi}^I(s) N_0^I(s))}. \quad (4.2)$$

In the elastic region the phase shift  $\delta_0^I$  is then related to the amplitude by  $\tan \delta_0^I = \text{Im} A_0^I / \text{Re} A_0^I$ . We have fitted all data for  $\delta_0^{1/2}$ ,  $a_0$  and  $\phi_0$  up to 1.31 GeV and for  $\delta_0^{3/2}$

up to 1.9 GeV simultaneously. The parameters for the fit are  $M_{K_0^*}$ ,  $c_d$ ,  $c_m$ ,  $c_{K\pi}^{1/2}$  and  $c_{K\pi}^{3/2}$ . Lacking further information, and to reduce the number of free parameters, we have set  $M_{S_1} = M_S = M_{K_0^*}$ , and we have used the large- $N_c$  estimate  $G_V = f_\pi/\sqrt{2} = 65.3$  MeV [9]. The latter value is in good agreement with the lowest-order results coming from the decay width of the  $K^*$  ( $\rho$ ) meson which yield  $G_V = 65$  (67) MeV and is also compatible with the original estimate  $G_V = 53$  MeV [8] which however already includes chiral loops. All other parameters have been taken from the Review of Particle Physics [45]. For the convenience of the reader we have compiled the constant input parameters in appendix D.

From our fits we observe that some of the parameters are strongly correlated and for example rather different values for the couplings of the scalar resonances can lead to similar fit quality. Thus it is necessary to have an idea what the values of  $c_d$  and  $c_m$  should be. In ref. [8] values for these parameters were estimated by assuming resonance saturation for the low-energy constants in the chiral Lagrangian. Taking the same approach with the most recent values for the low-energy constants [46, 47], and an average mass of the scalar octet  $M_S = 1.4$  GeV, we arrive at

$$|c_d| = 30 \pm 10 \text{ MeV}, \quad |c_m| = 43 \pm 14 \text{ MeV}, \quad (4.3)$$

with  $c_d c_m > 0$ , rather close to the original estimate in ref. [8]. For the error we have taken one third which is a typical error for large- $N_c$  estimates of chiral constants. The estimate  $M_S = 1.4$  GeV tacitly assumes that the correct  $I = 1$  scalar in this region is the  $a_0(1450)$ , and that the  $a_0(980)$  is generated dynamically [16, 20, 48–51]. Note however, that this question is controversial in the literature [52–54].<sup>3</sup>

As a first fit, we fix  $c_d$  and  $c_m$  to the central values presented in eq. (4.3) above. The remaining fit parameters are then found to be

$$M_{K_0^*} = 1.29 \text{ GeV}, \quad c_{K\pi}^{1/2} = -0.094, \quad c_{K\pi}^{3/2} = 1.703, \quad (4.4)$$

with a  $\chi^2 = 223.5/117 \text{ d.o.f.} = 1.91$ . The fits are performed with the program Minuit [55]. Since the fit parameters are highly correlated, we do not give statistical errors for the fit because they would underestimate the true uncertainties. We shall return to a discussion of the uncertainties below.

Next, the  $K\pi$  scattering data are fit with the constraint  $c_m = c_d$  for the couplings of the scalar resonances. This constraint is motivated from a calculation of the scalar form factor including resonances in the large- $N_c$  limit which will be presented in a subsequent

---

<sup>3</sup>For further discussion and references on this point see also the *note on scalar mesons* in the Review of Particle Physics [45].



publication [28]. Requiring the tree-level form factor to vanish at infinity, which should be a plausible assumption, in the case of one scalar resonance we find that  $c_d = c_m = f_\pi/2$ . For the corresponding fit the parameters take the values

$$\begin{aligned} M_{K_0^*} &= 1.19 \text{ GeV}, & c_d &= c_m = 45.4 \text{ MeV}, \\ c_{K\pi}^{1/2} &= -0.376, & c_{K\pi}^{3/2} &= 1.689. \end{aligned} \quad (4.5)$$

The  $\chi^2$  for this fit is  $210.6/116 \text{ d.o.f.} = 1.82$ . The resulting values of  $c_d$  and  $c_m$  turn out to be surprisingly close to the large- $N_c$  constraint  $f_\pi/2 = 46.2 \text{ MeV}$ .

Finally, we perform a fit leaving both  $c_d$  and  $c_m$  as free parameters. This fit results in

$$\begin{aligned} M_{K_0^*} &= 1.26 \text{ GeV}, & c_d &= 24.8 \text{ MeV}, & c_m &= 76.7 \text{ MeV}, \\ c_{K\pi}^{1/2} &= -0.191, & c_{K\pi}^{3/2} &= 1.700, \end{aligned} \quad (4.6)$$

and  $\chi^2 = 201.1/115 \text{ d.o.f.} = 1.75$ . Here,  $c_m$  turns out to be quite different from the central estimate given in eq. (4.3). However, comparing eqs. (4.4), (4.5) and (4.6) one sees that the  $\chi^2$  is around two for all three fits. Thus, the difference for the estimates of  $c_d$  and  $c_m$  gives an indication about the systematic uncertainties in their determination.

The fit result corresponding to eq. (4.6) is shown as the long-dashed line in figs. 1-4 for  $\delta_0^{1/2}$ ,  $a_0$ ,  $\phi_0$  and  $\delta_0^{3/2}$  respectively as a function of the invariant mass of the  $K\pi$  system  $M_{K\pi} = \sqrt{s}$ . The curves corresponding to the other two fits look similar. In figs. 2 and 3, data for  $a_0$  and  $\phi_0$  up to 1.6 GeV has been included already. The notation for the different data sets is as follows: ref. [38] full circles; ref. [39,40] full squares; ref. [41] full triangles; ref. [42] open circles; ref. [43] open squares; ref. [44] open triangles. As discussed above the errors for the data by refs. [38,41–44] have been increased by a factor of two. Concerning the quality of our fits we observe that the total  $\chi^2/\text{d.o.f.}$  is around two. This is due to the fact that the  $\chi^2$  for  $\delta_0^{3/2}$  individually is almost three. The individual  $\chi^2$  of  $\delta_0^{1/2}$ ,  $a_0$  and  $\phi_0$  are all close to one. Even removing the data for  $\delta_0^{3/2}$  above 1.3 GeV only reduces the  $\chi^2$  for  $\delta_0^{3/2}$  to about two. Thus we conclude that the unitarised chiral expression does not provide a fully satisfactory fit to the  $\delta_0^{3/2}$  data and that it somewhat prefers the older data. Nevertheless, compared to the conventional  $\chi$ PT result without unitarisation [29,30], the situation is much improved. For a comparison with the inverse amplitude method (IAM) see also ref. [56].

The somewhat unsatisfactory description of the  $I = 3/2$  data is probably due to the fact that there is no resonance contribution in the s-channel. Being pure background the chiral expressions are not expected to work very well at higher energies, because additional

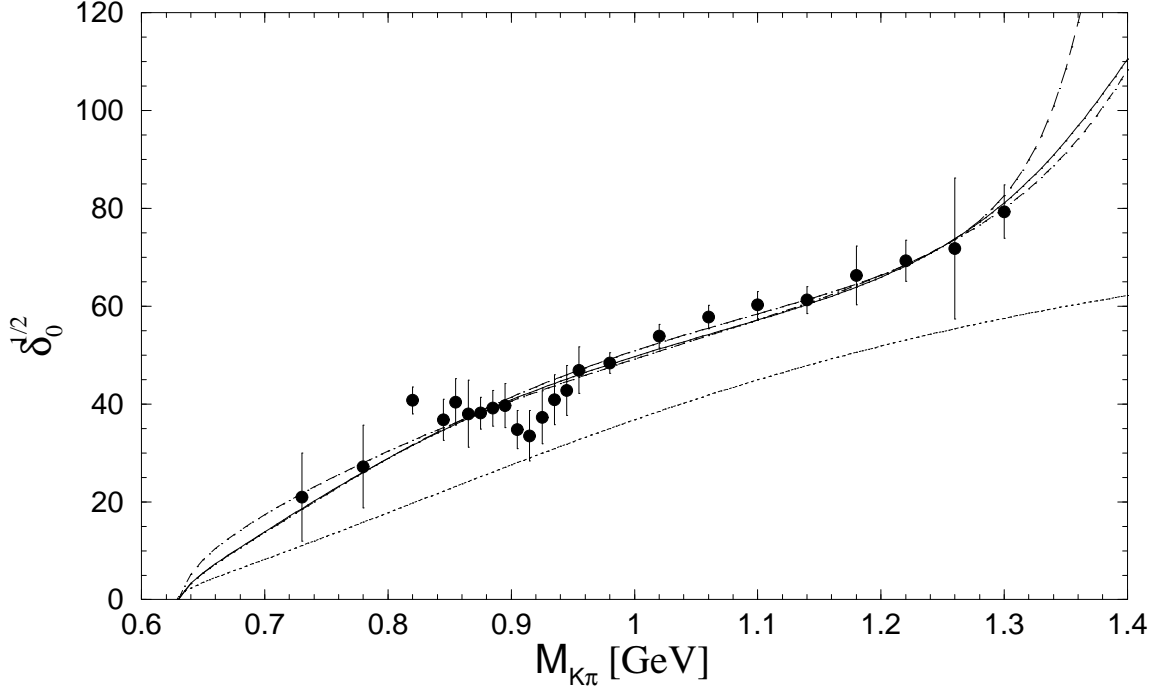


Figure 1: Elastic fits for  $\delta_0^{1/2}$ . Full circles: data of ref. [38]. Long-dashed line: fit of eq. (4.6); solid line: fit of eq. (4.10); short-dashed line: fit of eq. (4.13); dotted line: fit of eq. (4.14).

contributions not included in our low-energy description (e.g. higher-mass resonance exchanges in the  $t$  and  $u$  channels) could be important numerically. This is reflected in the fact that the contribution from unphysical cuts is much larger in the case of  $I = 3/2$  than for  $I = 1/2$ . However, the discrepancies among different sets of data, and the fact that the older  $I = 3/2$  data admits a better theoretical description, prevents us from drawing any clear conclusion. More precise experimental data are needed in this channel.

To further improve our overall fit for all data sets, we decided to use a unitarised background parametrisation for the  $\delta_0^{3/2}$  data:

$$\tan \delta_0^{3/2}(s) = \frac{\alpha q_{K\pi}(s)}{(1 + \beta q_{K\pi}^2(s) + \gamma q_{K\pi}^4(s))}, \quad (4.7)$$

where  $q_{K\pi}(s) = \sqrt{s} \sigma_{K\pi}(s)/2$  is the  $K\pi$  centre-of-mass momentum and  $\alpha$ ,  $\beta$  and  $\gamma$  are parameters of the ansatz. The parameter  $\alpha$  can be identified with the scattering length. Again, we perform the same three fits as with the chiral expression for the  $I = 3/2$  channel. First fixing  $c_d$  and  $c_m$  to the central values of eq. (4.3), we obtain

$$M_{K_0^*} = 1.28 \text{ GeV}, \quad c_{K\pi}^{1/2} = -0.130,$$

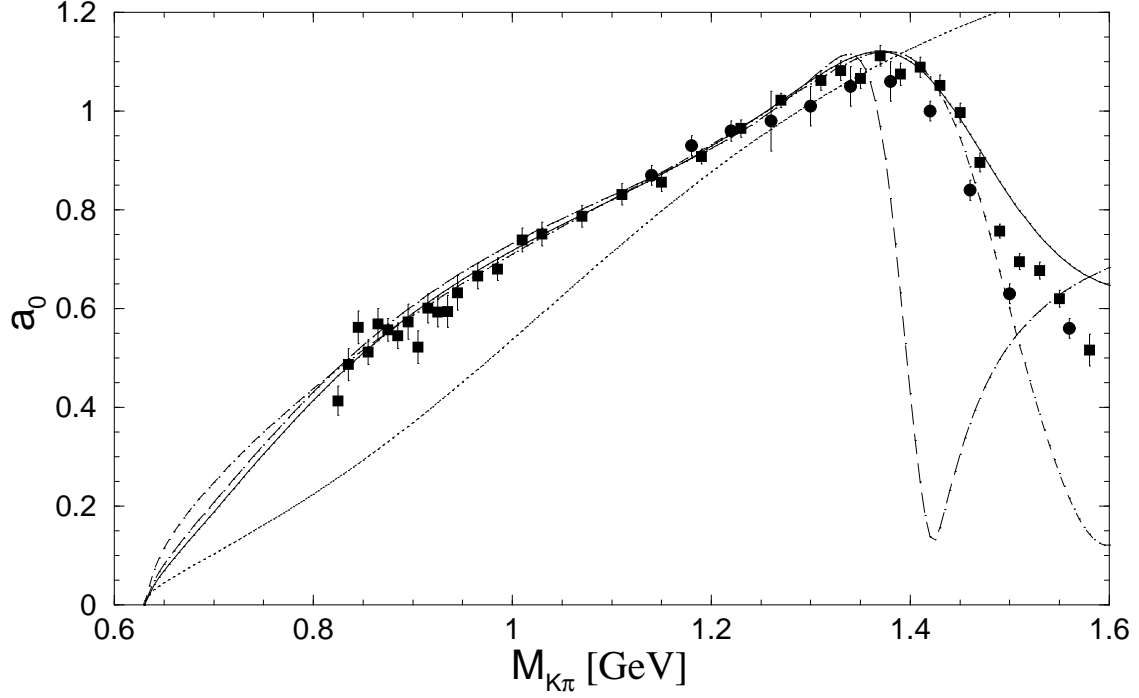


Figure 2: Elastic fits for  $a_0$ . Full circles: data of ref. [38]; full squares: data of ref. [39, 40]. Long-dashed line: fit of eq. (4.6); solid line: fit of eq. (4.10); short-dashed line: fit of eq. (4.13); dotted line: fit of eq. (4.14).

$$\alpha = -0.897 \text{ GeV}^{-1}, \quad \beta = -0.284 \text{ GeV}^{-2}, \quad \gamma = 1.945 \text{ GeV}^{-4}, \quad (4.8)$$

with a  $\chi^2 = 107.7/115 \text{ d.o.f.} = 0.94$ . The fit parameters imposing the constraint  $c_m = c_d$  are found to be

$$M_{K_0^*} = 1.19 \text{ GeV}, \quad c_d = c_m = 44.8 \text{ MeV}, \quad c_{K\pi}^{1/2} = -0.381, \\ \alpha = -0.859 \text{ GeV}^{-1}, \quad \beta = -0.580 \text{ GeV}^{-2}, \quad \gamma = 2.301 \text{ GeV}^{-4}, \quad (4.9)$$

and  $\chi^2 = 96.4/114 \text{ d.o.f.} = 0.85$ . Finally, leaving both  $c_d$  and  $c_m$  as free parameters yields

$$M_{K_0^*} = 1.36 \text{ GeV}, \quad c_d = 13.0 \text{ MeV}, \quad c_m = 85.4 \text{ MeV}, \quad c_{K\pi}^{1/2} = 0.200, \\ \alpha = -0.860 \text{ GeV}^{-1}, \quad \beta = -0.567 \text{ GeV}^{-2}, \quad \gamma = 2.283 \text{ GeV}^{-4}, \quad (4.10)$$

with  $\chi^2 = 90.5/113 \text{ d.o.f.} = 0.80$ . The last fit is shown as the solid curve in figs. 1-4. Compared to the fits with the chiral expression for the  $I = 3/2$  amplitude, the total  $\chi^2/\text{d.o.f.}$  is greatly improved. The individual  $\chi^2$  for  $\delta_0^{1/2}$  is around one and all other  $\chi^2$  are below one. The parameters  $\alpha$ ,  $\beta$  and  $\gamma$  have now replaced the parameter  $c_{K\pi}^{3/2}$  in the

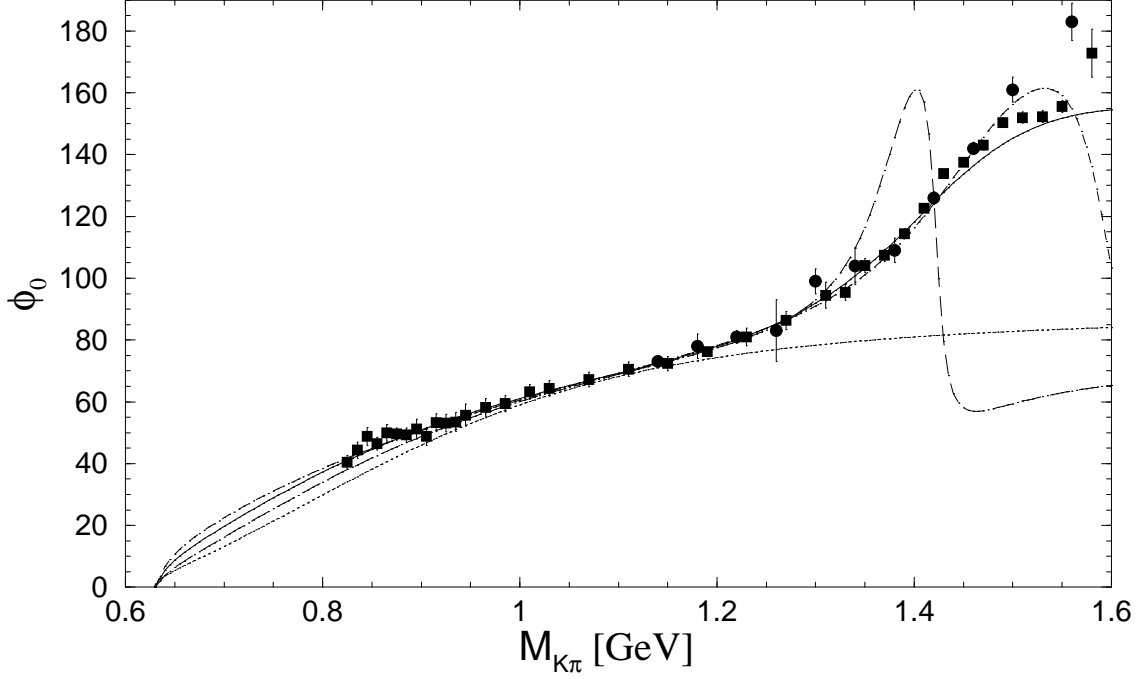


Figure 3: Elastic fits for  $\phi_0$ . Full circles: data of ref. [38]; full squares: data of ref. [39, 40]. Long-dashed line: fit of eq. (4.6); solid line: fit of eq. (4.10); short-dashed line: fit of eq. (4.13); dotted line: fit of eq. (4.14).

original parametrisation of the  $I = 3/2$  amplitude. We observe that for the fits with  $c_d$  unequal  $c_m$ , the  $K_0^*$  mass turns out to be somewhat larger than the results in eq. (4.5) and (4.9) and the value of  $c_{K\pi}^{1/2}$  depends very much on the other parameters. However, again rather different values of  $c_d$  and  $c_m$  lead to similar  $\chi^2$  implying sizeable uncertainties for these parameters.

Next, we compare our fits for the  $K\pi$  scattering amplitudes with the unitarised chiral expressions to a parametrisation for the  $I = 1/2$  amplitude with a  $K$ -matrix ansatz [31, 57, 58], keeping the background parametrisation of eq. (4.7) together with the parameters of eq. (4.10) for the  $I = 3/2$  amplitude. The conventional  $K$ -matrix ansatz is completely analogous to eq. (4.2),

$$A_0^{1/2}(s) = \frac{\sigma_{K\pi}(s) K_0^{1/2}(s)}{(1 - C(s) K_0^{1/2}(s))}, \quad (4.11)$$

where now  $C(s) = 16\pi \bar{J}_{K\pi}(s)$ , that is  $c_{K\pi}^{1/2} = 0$ , and

$$K_0^{1/2}(s) = \frac{g_R^2 M_R^2}{(M_R^2 - s)} + \frac{b(s - s_+)}{(1 + cs)}. \quad (4.12)$$

The  $K$ -matrix ansatz consists of a resonance term, with  $g_R$  being the coupling of the

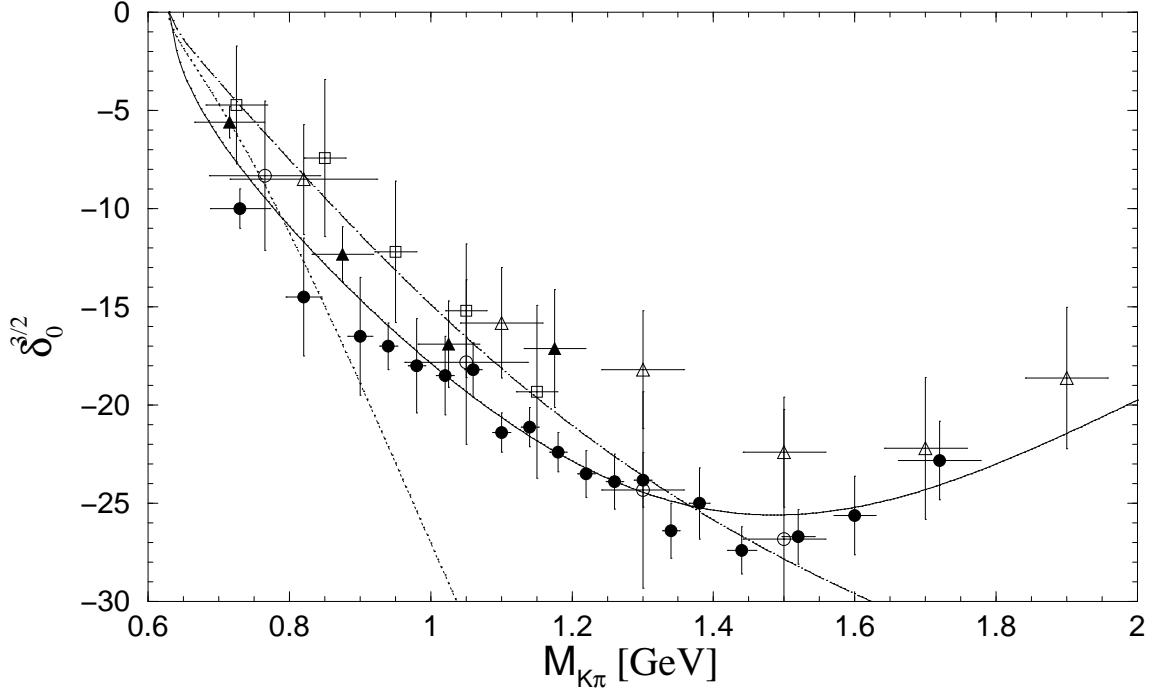


Figure 4: Elastic fits for  $\delta_0^{3/2}$ . The notation for the data sets is as follows: ref. [38] full circles; ref. [41] full triangles; ref. [42] open circles; ref. [43] open squares; ref. [44] open triangles. Long-dashed line: fit of eq. (4.6); solid line: fit of eq. (4.10); dotted line: fit of eq. (4.14).

resonance, and a background contribution. We have tried different forms of the background term, but the fit does not depend very much on this choice. In figures 1-3 the  $K$ -matrix fit corresponds to the short-dashed lines and the corresponding fit parameters take the values

$$\begin{aligned} M_R &= 1.32 \text{ GeV}, & g_R &= 0.628, \\ b &= 0.695 \text{ GeV}^{-2}, & c &= 0.172 \text{ GeV}^{-2}. \end{aligned} \quad (4.13)$$

The  $\chi^2 = 86.9/116 \text{ d.o.f.} = 0.75$  for this fit. Thus the fit quality is very similar to our fit (4.10) with the chiral expressions where we also used a pure background form for the  $I = 3/2$  amplitude.

Nevertheless, as can already be anticipated from the curvature of the two fits close to the  $K\pi$  threshold, the  $I = 1/2$  scattering lengths turn out to be somewhat different. Expanding our results close to threshold, we obtain  $\alpha_0^{1/2}(\text{K-matrix}) = 0.31 M_\pi^{-1}$ , whereas  $\alpha_0^{1/2}(\text{chiral}) = 0.18 M_\pi^{-1}$ , although the quality of the fit for  $I = 1/2$  is equally good. As has become conventional in the literature, we have expressed the scattering lengths

in units of  $M_\pi^{-1}$ . Even more dramatically, for the  $I = 3/2$  scattering lengths we find  $\alpha_0^{3/2}(\text{background}) = -0.12 M_\pi^{-1}$  and  $\alpha_0^{3/2}(\text{chiral}) = -0.05 M_\pi^{-1}$ . Our  $\chi$ PT results for the scattering lengths are in agreement with the order  $p^4$  calculation of ref. [29] (table 3). These findings show that reasonable fits to the experimental data can be obtained that spoil the  $\chi$ PT behaviour in the low-energy region close to the  $K\pi$  threshold. We conclude that the scattering lengths for S-wave  $K\pi$  scattering can only be extracted more reliably once better experimental data close to threshold become available.

Finally, to get some feeling about the importance of the resonance contribution and the real part of the unitarity corrections, as the dotted line in figs. 1-4, we display the leading order  $\chi$ PT result using a unitarisation according to the prescription:

$$\tan \delta_0^I = \sigma_{K\pi}(s) t_0^{I(2)}(s). \quad (4.14)$$

This prescription is equivalent to eq. (3.1) with the choice  $g(s) = i \sigma_{K\pi}(s)$  and  $N_0^I(s) = t_0^{I(2)}(s)$ . We should remark that this result is a parameter free prediction of lowest-order  $\chi$ PT. However, figs. 1-4 show that, except for  $\phi_0$  below roughly 1.2 GeV, resonance and the real part of unitarity corrections are required in order to obtain an acceptable description of the data.

## 5 Including the $K\eta$ and $K\eta'$ channels

Above roughly 1.3 GeV,  $K\pi$  scattering in the  $I = 1/2$  channel was found to be inelastic [38,39] with  $K\eta'$  being the first important inelastic channel. Therefore, in order to be able to describe  $K\pi$  scattering beyond 1.3 GeV, we need to include the  $K\eta'$  channel in the scattering amplitude in the framework of  $\chi$ PT with resonances. Although the  $K\eta$  channel was found to be unimportant, nevertheless, for consistency we have also included it in our analysis. The importance of the  $K\eta$  channel for our fits shall be further discussed below.

In the large- $N_c$  limit, the singlet  $\eta_1$  field becomes the ninth Goldstone boson and can then be incorporated with an extended  $U(3)_L \otimes U(3)_R$  chiral Lagrangian [59,60]. The large mass of the  $\eta'$  originates from the  $U(1)_A$  anomaly, which, although formally of  $\mathcal{O}(1/N_c)$ , is numerically important and cannot be treated as a small perturbation. It is possible to build a consistent combined chiral expansion in powers of momenta, quark masses and  $1/N_c$ , by counting the relative magnitude of these parameters as  $m_q \sim 1/N_c \sim \mathcal{O}(p^2)$  [61].

The physical states  $\eta$  and  $\eta'$  are mixtures of the SU(3) singlet and octet states  $\eta_1$  and  $\eta_8$ . If isospin-breaking effects are neglected, the mixing can be parametrised in terms of the mixing angle  $\theta$  usually defined by

$$\begin{aligned}
|\eta\rangle &= \cos\theta |\eta_8\rangle - \sin\theta |\eta_1\rangle, \\
|\eta'\rangle &= \sin\theta |\eta_8\rangle + \cos\theta |\eta_1\rangle.
\end{aligned}
\tag{5.1}$$

For our numerical analysis below, we shall use  $\sin\theta = -1/3 \approx -20^\circ$  which is in the ball-park of present day phenomenological values. Further details on  $\eta$ - $\eta'$  mixing in the framework of  $\chi$ PT with resonances can be found in appendix B. To be able to include the  $K\eta$  and  $K\eta'$  channels in the analysis of  $K\pi$  scattering we have to calculate the five scattering amplitudes  $T_{K\pi \rightarrow K\eta_i}$  and  $T_{K\eta_i \rightarrow K\eta_j}$  with  $i, j = 1, 8$ . The resulting expressions are rather lengthy and therefore, although representing one of our main results, have been relegated to appendix C. Eqs. (C.1) to (C.5) include the leading order  $p^2$  and the resonance contributions. So far, we have not calculated the order  $p^4$  loop contributions to the inelastic channels, but as will be explained in more detail below, the dominant contributions are accounted for by our unitarisation procedure. Using eq. (5.1), the five required amplitudes  $T_{K\pi \rightarrow K\eta}$ ,  $T_{K\pi \rightarrow K\eta'}$ ,  $T_{K\eta \rightarrow K\eta}$ ,  $T_{K\eta \rightarrow K\eta'}$  and  $T_{K\eta' \rightarrow K\eta'}$  can then easily be expressed in terms of  $T_{K\pi \rightarrow K\eta_i}$  and  $T_{K\eta_i \rightarrow K\eta_j}$ .

For a coupled channel analysis, our unitarisation procedure of section 3 has to be generalised and in particular eq. (3.1) has to be modified to a matrix equation. In the three-channel case,  $N(s)$  and  $g(s)$  become three by three matrices. Since in the following only S-wave  $K\pi$  scattering in the  $I = 1/2$  channel is considered, to simplify the notation we have dropped the corresponding indices in the expressions. Then the generalisation of eq. (3.1) takes the form [20, 21]

$$\tilde{t}(s) = N(s) \left[ 1 - g(s) N(s) \right]^{-1}, \tag{5.2}$$

with

$$N(s) = \begin{pmatrix} N_{K\pi \rightarrow K\pi}(s) & N_{K\pi \rightarrow K\eta}(s) & N_{K\pi \rightarrow K\eta'}(s) \\ N_{K\pi \rightarrow K\eta}(s) & N_{K\eta \rightarrow K\eta}(s) & N_{K\eta \rightarrow K\eta'}(s) \\ N_{K\pi \rightarrow K\eta'}(s) & N_{K\eta \rightarrow K\eta'}(s) & N_{K\eta' \rightarrow K\eta'}(s) \end{pmatrix}, \tag{5.3}$$

and

$$g(s) = \begin{pmatrix} g_{K\pi}(s) & 0 & 0 \\ 0 & g_{K\eta}(s) & 0 \\ 0 & 0 & g_{K\eta'}(s) \end{pmatrix}. \tag{5.4}$$

Several remarks are in order at this point. Because of time-reversal invariance,  $N(s)$  has to be symmetric. In addition, to satisfy unitarity  $N_{ij}^{-1}(s)$  needs to be real above the highest threshold of the channels  $i$  and  $j$ , and

$$\text{Im } g_i(s) = \theta(s - s_i) \sigma_i(s), \tag{5.5}$$

where  $i$  denotes the three channels  $K\pi$ ,  $K\eta$  or  $K\eta'$ ,  $s_i$  is the corresponding threshold, and the  $\sigma_i(s)$  are defined in analogy to eq. (3.5).

$N_{K\pi \rightarrow K\pi}$  is already given by eq. (3.2), and  $N_{K\pi \rightarrow K\eta}$ ,  $N_{K\pi \rightarrow K\eta'}$ ,  $N_{K\eta \rightarrow K\eta}$ ,  $N_{K\eta \rightarrow K\eta'}$  as well as  $N_{K\eta' \rightarrow K\eta'}$  result from the S-wave projection of the corresponding  $T$  amplitudes according to eq. (2.8). No subtractions have to be performed for these  $N(s)$  because we have not included the loop contributions to the  $K\eta$  and  $K\eta'$  channels explicitly. Therefore in this case  $N(s)$  is actually equal to  $t(s)$  (compare with eq. (3.2)). Finally, analogous to eq. (3.3),  $g_{K\eta}(s)$  and  $g_{K\eta'}(s)$  are written as

$$\begin{aligned} g_{K\eta}(s) &= 16\pi \bar{J}_{K\eta}(s) + c_{K\eta}, \\ g_{K\eta'}(s) &= 16\pi \bar{J}_{K\eta'}(s) + c_{K\eta'}, \end{aligned} \quad (5.6)$$

which satisfies eq. (5.5) automatically. Again,  $c_{K\eta}$  and  $c_{K\eta'}$  are arbitrary real constants.

As it stands, eq. (5.2) already includes the dominant part of the unitarity corrections which arise from the loop diagrams in  $\chi$ PT also for the inelastic channel. The imaginary parts are generated by the imaginary parts of  $g_{K\eta}(s)$  and  $g_{K\eta'}(s)$ . We have verified explicitly that the imaginary part generated from the leading contribution to the  $T_{K\pi \rightarrow K\eta_8}$  amplitude agrees with the imaginary part of the  $T_{K\pi \rightarrow K\pi}$  resulting from the  $\eta_8$  terms of eq. (2.5). Thus, when using eq. (2.5) in our numerical analysis, for consistency we have dropped the  $\eta_8$  contribution since it arises from the  $T_{K\pi \rightarrow K\eta_8}$  amplitude. On the other hand, the real parts of the unitarity corrections in the inelastic channels are not complete; the missing pieces are parametrised by the constants  $c_{K\eta}$  and  $c_{K\eta'}$ .

## 6 Fitting the inelastic case

For the inelastic case, the unitarised chiral expression corresponding to the S-wave  $I = 1/2$  amplitude  $A_0^{1/2}$  takes the form

$$A_0^{1/2}(s) = \sqrt{\sigma(s)} N(s) \left[ 1 - g(s) N(s) \right]^{-1} \sqrt{\sigma(s)}, \quad (6.1)$$

where

$$\sigma(s) = \begin{pmatrix} \sigma_{K\pi}(s) & 0 & 0 \\ 0 & \sigma_{K\eta}(s) & 0 \\ 0 & 0 & \sigma_{K\eta'}(s) \end{pmatrix}. \quad (6.2)$$

The  $K\pi \rightarrow K\pi$  contribution is obtained by taking the relevant matrix element of the matrix  $A_0^{1/2}(s)$ . If the  $K\eta$  and  $K\eta'$  contributions are removed one of course recovers the corresponding expression (4.2) for the single channel case.



Let us next discuss the situation of the experimental data in the inelastic region above 1.3 GeV. Because experimentally only the absolute value of the scattering amplitude can be determined, there are  $2^L$  discrete ambiguous solutions to the partial wave decomposition of the data where  $L$  is the maximal angular momentum that contributes at a given energy. These discrete ambiguities are apparent from the behaviour of the imaginary part of the amplitude (Barrelet) zeros  $z_i$  [62], if the scattering amplitude is expressed as a complex polynomial in  $z = \cos \theta$  where  $\theta$  is the scattering angle:

$$A(s, z) = \sum_{l=0}^L (2l+1) A_l(s) P_l(z) = f(s) \prod_{i=1}^L (z - z_i(s)). \quad (6.3)$$

The measurement of  $|A(s, z)|$  cannot determine whether  $z_i(s)$  or  $z_i^*(s)$  is a zero of  $A(s, z)$ ; thus the  $2^L$  ambiguity arises. Requiring the solutions to be smooth, it is possible to switch from one solution to another when a Barrelet zero  $z_i$  approaches the real axis. In the elastic region the ambiguity can be fixed from unitarity. However, in the inelastic region the behaviour of the Barrelet zeros has to be studied in detail.

Whereas in the experiment by Estabrooks et al. [38] a fourfold ambiguity arose above 1.5 GeV, because the imaginary parts of the two Barrelet zeros  $z_1$  and  $z_2$  were found to vanish within the experimental uncertainties, the group by Aston et al. [39] obtained an unambiguous solution up to 1.85 GeV. In the region between 1.86 GeV and 2.0 GeV Aston et al. found two solutions whereas above 2.0 GeV four solutions to the partial wave decomposition remained. Inspecting the signs of the imaginary parts of the  $z_i$  it is clear that the solution of Aston et al. below 1.85 GeV corresponds to solution B of Estabrooks et al. Since both experiments have similar statistics in our opinion the question whether the solution of Aston et al. in the region between 1.5 GeV and 1.85 GeV is the physical one, requires further corroboration. Nevertheless, we have decided to perform our fits to the experimental data by Aston et al. [39, 40] and solution B of Estabrooks et al. [38] up to 1.85 GeV with the unitarised chiral expressions.

In addition, we have also performed chiral fits to the other solutions of Estabrooks et al. [38] above 1.5 GeV. It is found that fits with reasonable values for the parameters can be obtained for data sets A, B and D whereas we were not able to find an acceptable fit for data set C. As far as the  $\chi^2$  is concerned, the best fit was obtained for data set A with  $\chi^2 = 1.70$ , the next best was data set B with  $\chi^2 = 1.86$  and finally data set D with  $\chi^2 = 2.57$ . Therefore, on the basis of these fits, we are unable to confirm that the solution found by the group of Aston et al. [39] is indeed the physical one. Note, however, that in ref. [63] arguments were put forward which entail that the solutions A and D of [38] are unphysical. This result, together with our fits, then favours solution B, in agreement with

the findings of ref. [39]. In what follows, we shall not discuss the additional solutions of Estabrooks et al. any further.

In the region of 1.9 GeV, the experiment by Aston et al. found a second scalar resonance in the S-wave channel. If we aim to describe the data up to such energies a second scalar nonet should be implemented in the unitarised chiral expressions. To this end we add in eqs. (2.4) and (C.1) to (C.5) a second nonet with degenerate mass  $M_{S'}$  and new scalar couplings  $c'_d$  and  $c'_m$  analogous to the first nonet. In addition we have also included two more vector octets with new couplings  $G_{V'}$  and  $G_{V''}$ . These couplings can be estimated from the decay rates  $K^*(1410) \rightarrow K\pi$  and  $K^*(1650) \rightarrow K\pi$  [45] with the results  $G_{V'} = 12$  MeV and  $G_{V''} = 23$  MeV, presumably with large errors. For our first fit as in section 4 we fix the values of  $c_d$  and  $c_m$  to the central values of eq. (4.3). Since we would like to have a good description for the  $I = 3/2$  channel up to 1.9 GeV, we chose to employ the unitarised background expression (4.7) as described in section 4. Using the chiral expressions also for  $I = 3/2$ , even including the higher scalar and vector resonances, did not provide acceptable fits in the region above 1.5 GeV. The fit parameters are then found to be

$$\begin{aligned} M_{K_0^*} &= 1.26 \text{ GeV}, & M_{S'} &= 2.17 \text{ GeV}, & c'_d &= 31.6 \text{ MeV}, & c'_m &= 46.9 \text{ MeV}, \\ c_{K\pi}^{1/2} &= 0.174, & c_{K\eta} &= -0.890, & c_{K\eta'} &= -0.722, \\ \alpha &= -0.760 \text{ GeV}^{-1}, & \beta &= -1.300 \text{ GeV}^{-2}, & \gamma &= 3.373 \text{ GeV}^{-4}, \end{aligned} \quad (6.4)$$

with a  $\chi^2 = 753.3/166 \text{ d.o.f.} = 4.54$ . The resulting  $\chi^2$  is found to be rather large indicating that the estimate of eq. (4.3) for  $c_d$  and  $c_m$  does not provide a good description of the data if inelastic channels and a second scalar resonance are included. We shall come back to a discussion of this point below. Analogous to section 4, the next fit is performed with the constraints  $c_m = c_d$  and  $c'_m = c'_d$ . The resulting fit parameters are

$$\begin{aligned} M_{K_0^*} &= 1.29 \text{ GeV}, & M_{S'} &= 1.86 \text{ GeV}, & c_d &= 25.8 \text{ MeV}, & c'_d &= 14.8 \text{ MeV}, \\ c_{K\pi}^{1/2} &= 0.179, & c_{K\eta} &= 0.504, & c_{K\eta'} &= -1.064, \\ \alpha &= -0.725 \text{ GeV}^{-1}, & \beta &= -1.817 \text{ GeV}^{-2}, & \gamma &= 4.385 \text{ GeV}^{-4}, \end{aligned} \quad (6.5)$$

with a  $\chi^2 = 470.9/166 \text{ d.o.f.} = 2.84$ . This fit is shown as the short-dashed line in figs. 5 and 6 for the modulus of the amplitude  $a_0$  and the phase  $\phi_0$  respectively. For comparison, in addition, as the dotted line we display the best fit for the elastic case of section 4, eq. (4.10).

Our notation for the shown data sets is as follows: solution B of Estabrooks et al. [38] full circles; solution A of Aston et al. [39, 40] full squares; solution B of [39, 40] empty

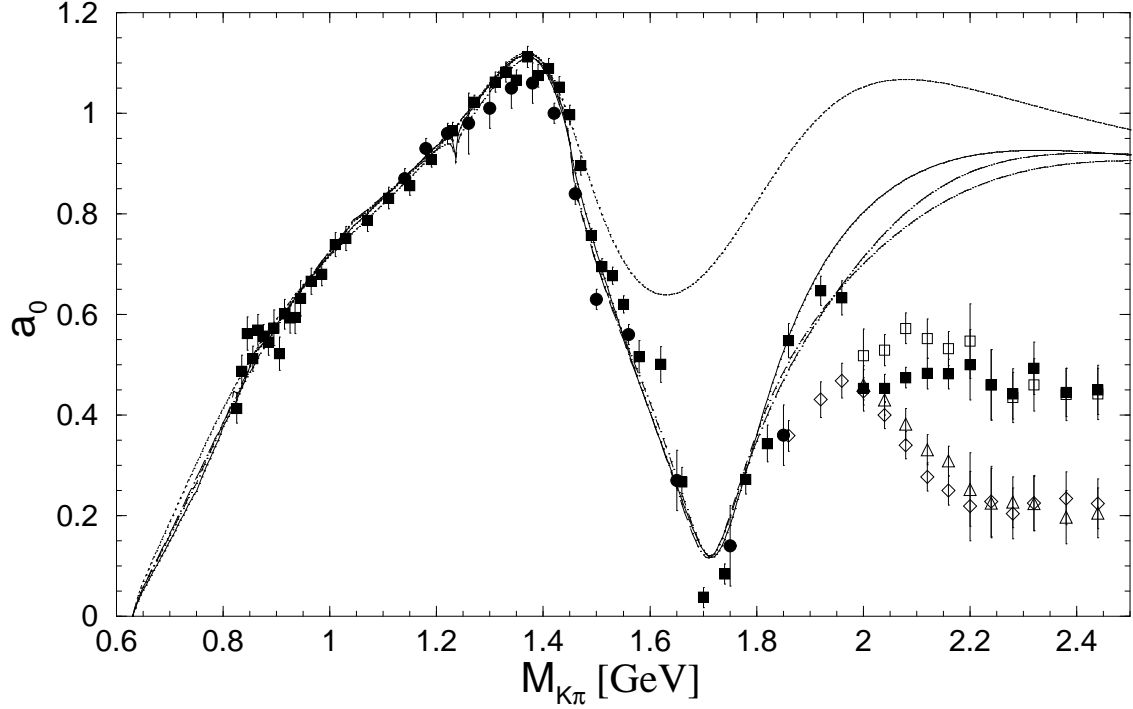


Figure 5: Inelastic fits for  $a_0$ . The notation for the data sets is as follows: solution B of [38] full circles; solution A of [39,40] full squares; solution B of [39,40] empty diamonds; solution C of [39,40] empty squares; solution D of [39,40] empty triangles. Dotted line: fit of eq. (4.10); short-dashed line: fit of eq. (6.5); solid line: fit of eq. (6.7); long-dashed line: fit of eq. (6.10).

diamonds; solution C of [39,40] empty squares; solution D of [39,40] empty triangles. Although in our fits we have only included data of Estabrooks et al. and Aston et al. up to 1.85 GeV where the partial wave analysis of Aston et al. gave a unique solution, in our figures all data up to 2.5 GeV are displayed for convenience. Data points where  $\phi$  is larger than  $180^\circ$  have not been included in the fit since they violate unitarity. This is easily seen from the relation

$$a_0 \sin(\phi_0) = \frac{1}{2} \left( 1 - \eta_0^{1/2} \cos(2\delta_0^{1/2}) \right) + \frac{1}{4} \left( 1 - \eta_0^{3/2} \cos(2\delta_0^{3/2}) \right), \quad (6.6)$$

which can be derived immediately by taking the imaginary part of eq. (4.1), because for  $0 \leq \eta_0^l \leq 1$  the right-hand side is always positive. This shows that solutions B and D of [39,40], also displayed in figs. 5 and 6, are unphysical.

Finally, we perform a fit leaving both  $c_d$  and  $c_m$  as free parameters but keeping the constraint  $c'_m = c'_d$  because otherwise we would have too many parameters, and the fit

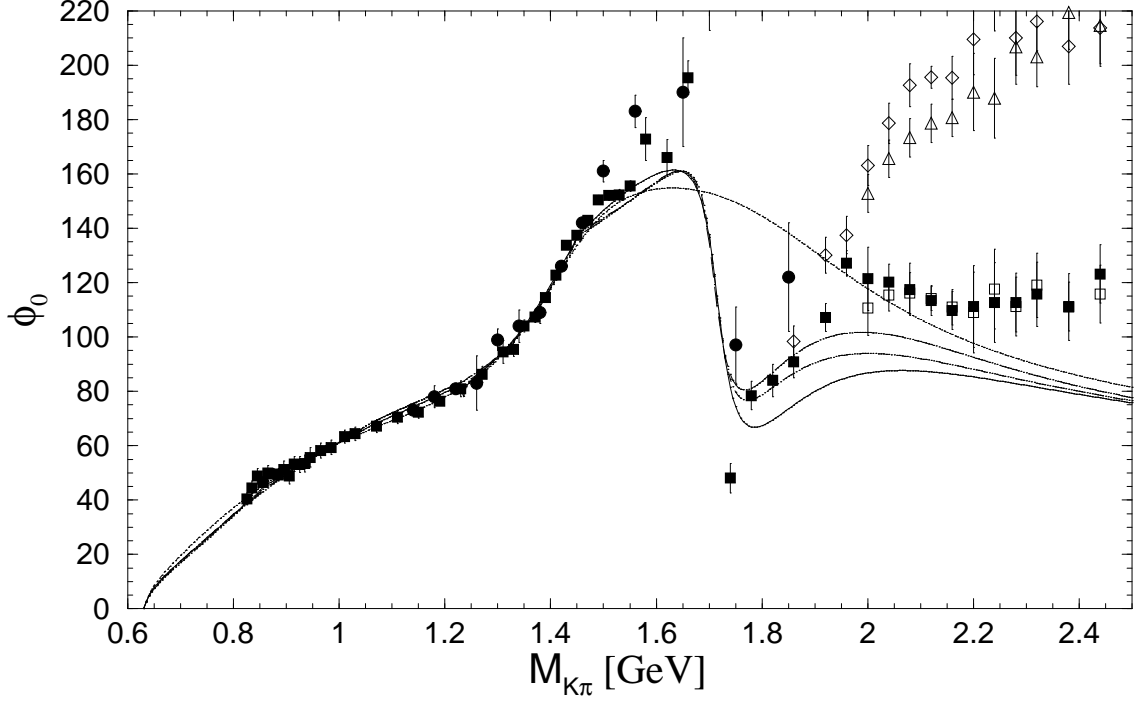


Figure 6: Inelastic fits for  $\phi_0$ . The notation for the data sets is as follows: solution B of [38] full circles; solution A of [39,40] full squares; solution B of [39,40] empty diamonds; solution C of [39,40] empty squares; solution D of [39,40] empty triangles. Dotted line: fit of eq. (4.10); short-dashed line: fit of eq. (6.5); solid line: fit of eq. (6.7); long-dashed line: fit of eq. (6.10).

would become unstable:

$$\begin{aligned}
M_{K_0^*} &= 1.30 \text{ GeV}, & M_{S'} &= 1.84 \text{ GeV}, & c_d &= 29.3 \text{ MeV}, & c_m &= 8.8 \text{ MeV}, \\
c'_d &= 13.1 \text{ MeV}, & c_{K\pi}^{1/2} &= 0.151, & c_{K\eta} &= 1.369, & c_{K\eta'} &= -1.388, \\
\alpha &= -0.816 \text{ GeV}^{-1}, & \beta &= -1.045 \text{ GeV}^{-2}, & \gamma &= 3.436 \text{ GeV}^{-4},
\end{aligned} \tag{6.7}$$

with a  $\chi^2 = 408.8/165 \text{ d.o.f.} = 2.48$ . The resulting amplitude and phase are shown as the solid line in figs. 5 and 6.

As for the fits in the elastic region presented in section 4, also in the inelastic case rather different values for the scalar couplings can lead to similar fit quality. Therefore, as in section 4, we next try to put further constraints on these couplings to single out physically sensible values. As will be discussed in a subsequent publication [28], the high-energy or short-distance behaviour of the scalar form factor can provide such constraints.

Requiring the tree-level form factor in the large- $N_c$  limit to vanish at infinite momentum transfer, for an arbitrary number of scalar resonances, one finds the following relations:

$$4 \sum_i c_{mi} c_{di} = f_\pi^2 \quad \text{and} \quad \sum_i \frac{c_{mi}}{M_{S_i}^2} (c_{mi} - c_{di}) = 0, \quad (6.8)$$

where  $M_{S_i}$ ,  $c_{di}$  and  $c_{mi}$  are the mass and the couplings of the  $i$ th resonance respectively.

In the case of two resonances, the short-distance constraints of eq. (6.8) can be used to express the couplings of the second resonance  $c'_d$  and  $c'_m$  in terms of the resonance masses and the couplings of the first resonance. For this fit, we find that  $c_{K\eta}$  is zero within the fit uncertainties. Thus we decided to set  $c_{K\eta} = 0$ . Fitting the remaining parameters, we obtain

$$\begin{aligned} M_{K_0^*} &= 1.41 \text{ GeV}, & M_{S'} &= 2.69 \text{ GeV}, & c_d &= 22.8 \text{ MeV}, \\ c_m &= 26.0 \text{ MeV}, & c_{K\pi}^{1/2} &= 0.178, & c_{K\eta'} &= 0.151, \end{aligned} \quad (6.9)$$

$$\alpha = -0.750 \text{ GeV}^{-1}, \quad \beta = -1.553 \text{ GeV}^{-2}, \quad \gamma = 4.041 \text{ GeV}^{-4},$$

with a  $\chi^2 = 505.6/167 \text{ d.o.f.} = 3.03$ . The values for  $c'_d$  and  $c'_m$  which resulted from the fit of eq. (6.9) are  $c'_d = 43.8 \text{ MeV}$  and  $c'_m = 35.3 \text{ MeV}$ . As our last fit, we employ the constraints (6.8) together with the reasonable assumption that  $c_m = c_d$  and again  $c_{K\eta} = 0$ . In this case, the fit parameters are found to be

$$\begin{aligned} M_{K_0^*} &= 1.40 \text{ GeV}, & M_{S'} &= 2.57 \text{ GeV}, & c_d &= 23.8 \text{ MeV}, \\ c_{K\pi}^{1/2} &= 0.173, & c_{K\eta'} &= 0.112, \end{aligned} \quad (6.10)$$

$$\alpha = -0.758 \text{ GeV}^{-1}, \quad \beta = -1.473 \text{ GeV}^{-2}, \quad \gamma = 3.929 \text{ GeV}^{-4},$$

with a  $\chi^2 = 507.1/168 \text{ d.o.f.} = 3.02$ . The resulting  $\chi^2$  is even slightly smaller than for the previous fit without the additional constraint  $c_m = c_d$ . For the couplings of the second resonance from this fit we obtain  $c'_d = c'_m = 39.6 \text{ MeV}$ . The latter fit is shown as the long-dashed line in figs. 5 and 6. Let us now come to a general discussion about the quality of the fits for the inelastic  $K\pi$  scattering amplitude.

Even for our best fit of eq. (6.7), the resulting  $\chi^2$  is larger than two. In our opinion the reason for this is twofold. On the one hand, the systematic uncertainties for the data above 1.3 GeV seem to be underestimated. This is seen if the data are fit with a Breit-Wigner-resonance plus background ansatz [39]. Even increasing the number of parameters in the parametrisation of the background, the lowest  $\chi^2$  is found to be of the order of 1.5. On the other hand, additional inelastic channels like  $K\pi\pi\pi$  are still missing in our

theoretical expressions. This could also lead to deficiencies in the description of the data in the higher-energy region. However, in view of our first remark, the experimental data are described rather well which in turn implies that additional inelastic channels should not be too important. This is supported by the fact that those contributions are of higher order in the chiral and  $1/N_c$  expansions and should be suppressed.

Comparing the various fits for the inelastic channel, like in section 4 one finds that similar fit quality can be achieved with rather different values for the couplings of the scalar resonances. In view of this fact it seemed desirable to put further constraints on these couplings from general considerations. These are provided by the short-distance constraints (6.8) which arise if one requires that the tree-level scalar form factor in the large- $N_c$  limit should vanish at infinite momentum transfer. For this reason, we believe that the fits of eqs. (6.5) and especially (6.10) are physically most sensible, although for the description of the data, the fits of eqs. (6.7) and (6.9) lead to very similar results.

As has been mentioned at the beginning of section 5, experimentally it was observed that the  $K\eta$  channel is not important for S-wave  $K\pi$  scattering up to 2 GeV. Thus, to get a further understanding about which of our fits is most physical, let us investigate how sensitive the fits are concerning a removal of the  $K\eta$  channel. For simplicity, we just consider the fits of eqs. (6.5) and (6.10).

If the  $K\eta$  channel is removed in the fit of eq. (6.5), the  $\chi^2$  is increased to  $\chi^2 = 664/167 \text{ d.o.f.} = 3.98$ . On the other hand, if an analogous fit without the  $K\eta$  channel and the constraints  $c_m = c_d$  and  $c'_m = c'_d$  is performed, a fit with similar quality than (6.5) can be obtained:

$$\begin{aligned} M_{K_0^*} &= 1.29 \text{ GeV}, & M_{S'} &= 1.94 \text{ GeV}, & c_d &= 27.9 \text{ MeV}, \\ c'_d &= 20.1 \text{ MeV}, & c_{K\pi}^{1/2} &= 0.173, & c_{K\eta'} &= -0.860, \\ \alpha &= -0.846 \text{ GeV}^{-1}, & \beta &= -0.917 \text{ GeV}^{-2}, & \gamma &= 3.403 \text{ GeV}^{-4}, \end{aligned} \quad (6.11)$$

with a  $\chi^2 = 479.6/167 \text{ d.o.f.} = 2.87$ . Putting back the  $K\eta$  channel for these fit parameters only increases the  $\chi^2$  to  $522/167 \text{ d.o.f.} = 3.13$ . Therefore, as far as the sensitivity with respect to the  $K\eta$  channel is concerned, the fit (6.11) is preferred over the fit (6.5).

Performing the same exercise of removing the  $K\eta$  channel in the fit of eq. (6.10), the  $\chi^2$  is even slightly decreased to  $488/168 \text{ d.o.f.} = 2.90$ . In this sense there is some indication that the parameter set of eq. (6.10) is the most physical of our fits to the S-wave  $K\pi$  scattering amplitude.

In the original publications where the inclusion of resonances in the framework of  $\chi$ PT was worked out [8,9], it was suggested that the order  $p^4$  coupling constants  $L_5$  and  $L_8$  are

saturated by the contribution of the scalar octet resonances to a very good approximation. In the case of two resonances these contributions are given by:

$$L_5^S = \frac{c_d c_m}{M_S^2} + \frac{c'_d c'_m}{M_{S'}^2} \quad \text{and} \quad L_8^S = \frac{c_m^2}{2M_S^2} + \frac{c'_m{}^2}{2M_{S'}^2}. \quad (6.12)$$

Thus, assuming resonance saturation of  $L_5$  and  $L_8$  and using our fit parameters we are in a position to calculate these chiral couplings. Taking the fit of eq. (6.10) including the short-distance constraint as an example, we then find

$$L_5^S = 0.52 \cdot 10^{-3} \quad \text{and} \quad L_8^S = 0.26 \cdot 10^{-3}, \quad (6.13)$$

in good agreement to the most recent determination of these constants [46, 47] and also supporting lower values than were found in earlier estimates. The fact that in this approach we obtain  $L_5 = 2L_8$  follows immediately from the second constraint of eq. (6.8). Similar values for  $L_5$  and  $L_8$  are also obtained for the other fits to the inelastic scattering amplitude.

## 7 The $T$ -matrix poles

In the energy region above the  $K\pi$  threshold and below roughly 2 GeV, the possible presence of three scalar resonances in the S-wave  $I = 1/2$  channel has been discussed in the literature. The only one which is clearly observed in the experimental data is the  $K_0^*(1430)$  [38, 39]. Less obvious is the existence of the  $K_0^*(1950)$  resonance [39] in the region around 2 GeV, and concerning the third, the lowest-lying  $\kappa$  meson [19, 20, 64–69], there has been some controversy in recent years [54, 70, 71].

We now address this problem by searching for possible poles of the matrix  $\tilde{t}(s)$ , eq. (5.2), associated with these resonances in the nearby unphysical Riemann sheets. As discussed above, the influence of the  $K\eta$  threshold in the S-wave  $I = 1/2$  partial wave amplitude was found to be very small and hence, in order to simplify the notation, we shall label the different Riemann sheets as if we had only a two channel problem with  $K\pi$  and  $K\eta'$ . In this way, the first or physical Riemann sheet is indicated by  $(+, +)$ , the second one by  $(-, +)$ , the third one by  $(-, -)$  and the fourth by  $(+, -)$ . The signs between brackets refer to the sign ambiguity present in the definition of the modulus of the centre-of-mass three-momentum due to the presence of the square root of eq. (3.5). In this way, the ‘+’ sign indicates that the imaginary part of the modulus of the three-momentum is always positive in the whole  $s$ -plane and the ‘−’ sign refers to the contrary. The sign between brackets on the left side corresponds to the  $K\pi$  system and the one on the right side to the  $K\eta'$  state. We start by investigating the pole positions for our preferred fit of eq. (6.10).

At the end of this section, we shall also compare with the pole positions found for some of the other fits obtained in sections 4 and 6.

The nearby Riemann sheet for the  $\kappa$  resonance is the second one, since this state should appear with a mass much lower than the threshold of the  $K\eta'$  channel. In fact, we find a pole in the second Riemann sheet  $(-, +)$  at

$$\sqrt{s_\kappa} = (708 - i 305) \text{ MeV} . \quad (7.1)$$

This pole position is very similar to the one found in ref. [20] at  $(779 - i 330) \text{ MeV}$ .<sup>4</sup> Note that the main differences between ref. [20], applied to the specific case of S-wave  $I = 1/2$  scattering, and the present work are that in the former unphysical cut contributions were not included, the  $K\eta'$  channel was not considered (although its influence below 1.3 GeV is very smooth), and the short distance constraints were not imposed. However, in the present work, although we have included all this information, the pole (7.1) corresponding to the  $\kappa$  resonance appears in a similar position to the one found in ref. [20]. (We are talking about a resonance with a width of about 600 MeV; hence small variations in its mass and width under realistic changes in the dynamical input are completely natural.) These findings are expected since in ref. [20] it was estimated that the contribution from the unphysical cuts in the physical region below 0.8 GeV amounts just to a few percent. Thus the stability of the expansion in the physical region in terms of the unphysical cut contributions at these energies seems to be justified.

We have checked that this pole is of dynamical origin, that is, it is generated through the strong rescattering (unitarity loops) of the  $K\pi$  channel. For instance, this pole survives when one removes all the explicit tree-level resonant contributions, as was already established in ref. [20]. Because of this fact and also because the  $\kappa$  is a very wide resonance, which implies that its contribution to the physical data is rather soft, one can expect that the existence and properties of this pole are rather model dependent. This is basically what is observed in the recent work [71], where a different conclusion has been obtained. However, contrary to what is concluded in this reference, the model dependence does not imply that the  $\kappa$  does not exist. It means that a good dynamical model, based on first principles, is required, in order to assess the question whether there is or is not a pole to be associated with the  $\kappa$  resonance. This is in fact one of the aims of the present work.

Before finishing the general discussion with respect to the  $\kappa$ , let us remind that this pole, together with the  $\sigma(500)$ ,  $a_0(980)$  and a strong contribution to the  $f_0(980)$ , gives

---

<sup>4</sup>Employing the pole position one can identify the real part with the mass of the resonance and the modulus of the imaginary part with one half of its width. For narrow objects, this identification agrees with the Breit-Wigner resonance picture.



rise to the lightest scalar nonet [20]. In this work, the whole  $J^{PC} = 0^{++}$  nonet was found to be of dynamical origin, that is, due to the strong rescattering in this channel between the pseudoscalars from the lowest order  $\chi$ PT amplitudes. In fact, taking the results of ref. [20], it is possible to go to the SU(3) limit by considering the limit of equal masses for the pseudoscalars. In that way, one can see how the poles move continuously giving rise to an octet of degenerate scalar resonances plus a singlet.

Now we turn to the  $K_0^*(1430)$  resonance. This state is clearly seen as a steep rise in the phase, figs. 3 and 6, and as a peak structure in the modulus of the amplitude, figs. 2 and 5. The threshold of the  $K\eta'$  is very close to the expected mass of this resonance and hence we should investigate the pole positions both in the second  $(-, +)$  and in the third  $(-, -)$  Riemann sheet, which are the nearby ones in this case. We find the following pole positions for the fit (6.10):

Sheet	Pole Position	
$(-, +)$	$\sqrt{s}_{K_0^*(1430)} = (1450 - i 142) \text{ MeV}$	(7.2)
$(-, -)$	$\sqrt{s}_{K_0^*(1430)} = (1358 - i 243) \text{ MeV}$	

There is a clear dependence in the position of the pole with respect to the sheet. This is expected since the resonance, although originating from a tree level pole included around 1.4 GeV, has strong unitarity corrections and is also influenced by the nearby  $K\eta'$  threshold. In any case, the pole position found in the second Riemann sheet is very close to the effective values of the mass  $1429 \pm 4 \pm 5 \text{ MeV}$  and width  $287 \pm 10 \pm 21 \text{ MeV}$  given in refs. [39], deduced from a simple Breit-Wigner fit to the experimental data. It is worth to stress that this is the lightest preexisting  $I = 1/2$  scalar state.

Finally, some structure in the phase and modulus of the amplitude around 1.7–1.9 GeV is also observed in the experimental data by Aston et al. [39] (solutions A and C of ref. [39] in figs. 5 and 6, reminding that solutions B and D of this reference are unphysical). In ref. [39], an additional simple Breit-Wigner plus background fit was performed for this energy region only, establishing the presence of the  $K_0^*(1950)$  resonance. The effective mass and width given in that work varied as a function of the chosen solution for the partial wave amplitude. For solution A, a mass of  $1934 \pm 8 \pm 20 \text{ MeV}$  and a width of  $174 \pm 19 \pm 79 \text{ MeV}$  was found, whereas for the unphysical solution B the mass was  $1955 \pm 10 \pm 8 \text{ MeV}$  and the width  $228 \pm 34 \pm 22 \text{ MeV}$ . As explained above, our fits were performed including data from ref. [39] up to 1.85 GeV. In this energy interval the solution of ref. [39] is unambiguous and in fact our fits also give rise to a pole in the energy region around 1.9 GeV. For the fit

(6.10), the poles in the nearby third  $(-, -)$  and in the second Riemann sheet  $(-, +)$  are:

Sheet	Pole Position	
$(-, -)$	$\sqrt{s_{K_0^*(1950)}} = (1731 - i 147) \text{ MeV}$	(7.3)
$(-, +)$	$\sqrt{s_{K_0^*(1950)}} = (1908 - i 27) \text{ MeV}$	

One can see a large variation in the position of this pole from one sheet to another indicating a strong departure from the simple Breit-Wigner resonance behaviour. Furthermore, we have checked that this resonance is an interplay between the underlying dynamics discussed in the previous sections and rescattering effects.<sup>5</sup> On the other hand, while the mass from the pole position in the second sheet is closer to the effective one of ref. [39], the width from the pole in the third sheet is closer to the one given in that work.

Let us now come to a comparison of the pole positions resulting from different fits of sections 4 and 6. In table 1, we give the poles corresponding to the previously discussed resonances in the second sheet for the fits: (6.10), (6.11), (6.7), (4.4), (4.9) and (4.10). Since the last three fits correspond to the elastic case of section 4, only the resonances  $\kappa$  and  $K_0^*(1430)$  are considered for them. In this table, we also show the residua of the poles associated with the different channels. They are defined by the limit:

$$r_i \equiv \lim_{s \rightarrow s_R} \sqrt{|(s - s_R)T_{ii}|} \quad (7.4)$$

with  $i$  referring to the considered channel ( $i = 1, 2, 3 \leftrightarrow K\pi, K\eta, K\eta'$ ) and  $s_R$  is the location of the pole for the resonance in question. The residua presented in table 1 show that the  $\kappa$  couples strongly to the  $K\pi$  state and much less to the  $K\eta$  and  $K\eta'$  channels. The  $K_0^*(1430)$  and  $K_0^*(1950)$  couple strongly with the  $K\pi$  and  $K\eta'$  states with comparable strengths in both cases. On the other hand, the coupling of these resonances with the  $K\eta$  state is much weaker.

When comparing the different fits in table 1, one sees that the properties of the  $\kappa$  meson are rather stable when changing from one fit to another. For the  $K_0^*(1430)$  one observes a common trend in the inelastic fits, as well as in the elastic one of eq. (4.10), to give a pole around  $(1.44 - i 0.15) \text{ GeV}$ . There is, however, a large difference between the pole position and the residua  $r_1$  corresponding to the elastic fit (4.9) and the ones given by the inelastic fits. On the other hand, the values from the fit (4.4) lie in an intermediate region. We will further discuss these points after introducing table 2 below.

For the  $K_0^*(1950)$  the situation is more unstable when comparing different fits, particularly with respect to the imaginary part of the pole position in the second sheet. However,

---

<sup>5</sup>The bare parameters of the second resonance change considerably for the different fits and in fact for the fit (6.10) the bare mass is as high as 2.57 GeV.

Sheet:( $-$ , $+$ )	$\kappa$	$K_0^*(1430)$	$K_0^*(1950)$
(6.10) $r_{1,2,3}$	(708 $- i$ 305) MeV 4.51, 2.36, 1.68	(1450 $- i$ 142) MeV 4.86, 1.07, 4.12	(1908 $- i$ 27) MeV 5.01, 0.73, 5.97
(6.11) $r_{1,2,3}$	(694 $- i$ 329) MeV 4.83, 2.78, 1.72	(1447 $- i$ 160) MeV 5.32, 1.29, 4.71	(1966 $- i$ 50) MeV 5.75, 0.99, 7.03
(6.7) $r_{1,2,3}$	(714 $- i$ 301) MeV 4.31, 1.55, 1.19	(1429 $- i$ 146) MeV 4.82, 0.85, 2.67	(1880 $- i$ 112) MeV 4.76, 0.91, 4.20
(4.4) $r_1$	(701 $- i$ 320) MeV 4.79	(1437 $- i$ 70) MeV 3.53	Elastic Case
(4.9) $r_1$	(709 $- i$ 306) MeV 4.74	(1386 $- i$ 48) MeV 2.85	Elastic Case
(4.10) $r_1$	(684 $- i$ 279) MeV 4.10	(1407 $- i$ 140) MeV 4.21	Elastic Case

Table 1: A collection of the pole positions and residua  $r_i$  for the fits of eqs. (6.10), (6.11), (6.7), (4.4), (4.9) and (4.10) in the second Riemann sheet. The  $r_i$  are given in units of  $M_\pi$ .

as can be seen in figs. 5 and 6, all the inelastic fits result in rather similar curves. This clearly implies that the role of the  $K_0^*(1950)$  is hidden by a very large background and hence one needs a very precise approach for such large energies around 2 GeV in order to extract the resonance-pole parameters. This is clearly out of the scope of the present paper because for such high energies, additional multiparticle states can play a significant role and also the contributions of the unphysical cuts become increasingly large. Let us note that for the fit (6.7) the pole position corresponding to this resonance is very similar to the mass and width obtained in ref. [39], the only reference considered in the Review of Particle Physics [45] for the  $K_0^*(1950)$ .

Table 2 is analogous to table 1, but now considering the third Riemann sheet ( $-$ ,  $-$ ). Therefore, in this second table, we do not show the  $\kappa$  resonance and we only consider inelastic fits. The third sheet is in principle the closest one to the physical  $s$ -axis when one is well above the  $K\eta'$  threshold. This is clearly the situation for the  $K_0^*(1950)$ . For the  $K_0^*(1430)$  one also needs to consider the second sheet ( $-$ ,  $+$ ) discussed above, since we are very close to the  $K\eta'$  threshold. From table 2, one infers that for this latter case the pole associated with the  $K_0^*(1430)$  in the third sheet is very broad, but with similar residua to the one in the second sheet, and thus one would expect that the pole driving the effects of the  $K_0^*(1430)$  on the physical axis should correspond to the one in the second sheet. In

Sheet:(-, -)	$K_0^*(1430)$	$K_0^*(1950)$
(6.10)	$(1358 - i 243)$ MeV	$(1731 - i 147)$ MeV
$r_{1,2,3}$	5.56, 1.65, 4.41	3.67, 0.24, 4.84
(6.11)	$(1299 - i 255)$ MeV	$(1700 - i 151)$ MeV
$r_{1,2,3}$	5.52, 1.44, 4.07	3.79, 0.24, 4.62
(6.7)	$(1394 - i 188)$ MeV	$(1772 - i 172)$ MeV
$r_{1,2,3}$	5.18, 0.84, 3.19	4.24, 0.58, 4.42

Table 2: A collection of the pole positions and residua  $r_i$  for the inelastic fits of eqs. (6.10), (6.11) and (6.7) in the third Riemann sheet. The  $r_i$  are given in units of  $M_\pi$ .

fact, the masses and widths of the  $K_0^*(1430)$  derived from the second sheet poles listed in table 1, corresponding to the inelastic fits and also to the elastic one (4.10), are in fairly good agreement with the effective values of ref. [39].

Concerning the  $K_0^*(1950)$  resonance poles, there is no clear and simple criterion in order to decide which pole, the one in the second or in the third sheet, is the leading one. In fact, when comparing with the experimental data of solutions A and C of ref. [39], fig. 5, one observes a dip in the modulus of the amplitude around 1.7 GeV. This precisely corresponds to the real part of the pole position corresponding to the  $K_0^*(1950)$  in the third Riemann sheet, table 2. On the other hand, when looking at the phase shifts for the same solutions in fig. 6, one sees a local maximum around 1.9 GeV, which coincides with the real part of the poles in the second sheet, table 1. Furthermore, as discussed above, in the region of the  $K_0^*(1950)$  there is a large background that could mimic the effects of the broad and lighter pole found in the third sheet.

## 8 Conclusions

S-wave scattering of the pseudoscalar Goldstone bosons is a good testing ground for our understanding of strong interactions in the non-perturbative region. At low energies, the Goldstone dynamics is constrained by the chiral symmetry properties of QCD. The  $\chi$ PT Lagrangian contains all relevant information on the infrared singularities (thresholds, cuts, etc.), which allows to reconstruct the scattering S-matrix elements up to local subtraction polynomials. The structure of these local terms is also governed by chiral symmetry, but their coefficients, the chiral couplings, encode the short-distance information.

The  $\chi$ PT predictions can be extrapolated to higher energies by taking into account

the leading massive singularities, i.e. incorporating the lightest resonance poles through a chiral-symmetric Effective Field Theory with resonance fields as explicit degrees of freedom [8,9]. Combined with large- $N_c$  arguments to organise a well-defined perturbative approach, this procedure provides a good understanding of many low and intermediate energy phenomena. However, it is not enough to achieve a correct description of the scalar sector, because the S-wave rescattering of two pseudoscalars is very strong, making necessary to perform a resummation of chiral-loop corrections in order to satisfy unitarity [17–21].

In this paper, we have tried to describe the S-wave  $K\pi$  scattering up to 2 GeV, through a unitarisation of the resonance chiral Lagrangian predictions. In the elastic region a reasonably good description can be achieved for the dominant  $I = 1/2$  amplitude, which satisfies all low-energy and high-energy constraints. However, the more exotic  $I = 3/2$  sector remains problematic, in spite of the clear improvement provided by the unitarisation procedure. Being pure background (no resonances), and with very large contributions from crossed channel dynamics, it is more difficult to get a good high-energy extrapolation for the  $I = 3/2$  amplitude since many missing small corrections could be numerically important. Nevertheless, the present discrepancies among different sets of data prevent us from reaching any firm conclusion; in fact, the older  $I = 3/2$  data appears to be better described within the chiral framework.

Above roughly 1.3 GeV, the  $I = 1/2$  amplitude contains inelastic contributions. We have incorporated the leading two-body  $K\eta$  and  $K\eta'$  modes, through a coupled channel analysis. The necessary input are the five independent  $T_{K\pi \rightarrow K\eta_i}$  and  $T_{K\eta_i \rightarrow K\eta_j}$  amplitudes, which we have computed at the required order.

The inelastic fit faces the problem of a very unsatisfactory experimental status. The data only determines the absolute value of the scattering amplitude, leaving  $2^L$  discrete ambiguous solutions to the partial wave decomposition with  $L$  being the maximal angular momentum contributing at a given energy. Moreover, different experiments give rise to different solutions making rather unclear the comparison with theory. Even the masses and widths of the dominant scalar resonances are not clearly established.

We have combined the known theoretical ingredients in order to see which experimental solutions are preferred. Up to 1.85 GeV, the Aston data [39,40] corresponds to solution B of Estabrooks [38]. Arguing that this should be the physical solution, we have performed several fits in the respective region and studied their behaviour at higher energies where the data ambiguities are more severe. Although some of the solutions of ref. [39] for energies higher than 1.85 GeV are shown to be unphysical, since they violate unitarity and can be discarded, the large experimental errors do not allow to unambiguously select the physical one.

A similar fit quality could be achieved with rather different values of the input parameters. Nevertheless, when imposing the high-energy constraints discussed above, definite values for some of the parameters can be given. In addition, assuming saturation of the low-energy constants  $L_5$  and  $L_8$  by scalar-resonance contributions, we were able to estimate values for these parameters which are compatible with the very recent work [46, 47]. We have also used our fits to study the position of the T-matrix poles in the complex plane, aiming to determine the mass and width of the dominant scalar resonances.

Clearly, better experimental data are needed. Our results provide a convenient theoretical framework to be used in future experiments for analysing the data and resolving possible ambiguities. Even with all present shortcomings, our analysis considerably improves the knowledge of the S-wave  $K\pi$  scattering amplitude. In a forthcoming publication [28], we will use this information to perform a detailed investigation of the  $K\pi$  scalar form factor up to 2 GeV. We expect that this could help to improve the determination of the strange quark mass from QCD sum rules for the strangeness-changing scalar current [22–27].

## Acknowledgements

We would like to thank B. Ananthanarayan and P. Büttiker for calling our attention to ref. [63] as well as H. G. Dosch and U.-G. Meißner for critically reading the manuscript. This work has been supported in part by the German-Spanish Cooperation Agreement HA97-0061, by the European Union TMR Network EURODAFNE (ERBFMX-CT98-0169), and by DGESIC (Spain) under the grants no. PB97-1261 and PB96-0753. M. J. would like to thank the Deutsche Forschungsgemeinschaft for support.

# Appendices

## A Loop functions

For completeness, we tabulate here the one-loop functions [3] appearing in the unitarity chiral correction of eq. (2.5). The basic integral is given by:

$$\begin{aligned}\bar{J}_{PQ}(s) &\equiv -\frac{1}{16\pi^2} \int_0^1 dx \log \left[ \frac{M_P^2 - sx(1-x) - \Delta_{PQ}x}{M_P^2 - \Delta_{PQ}x} \right] \\ &= \frac{1}{32\pi^2} \left\{ 2 + \left( \frac{\Delta_{PQ}}{s} - \frac{\Sigma_{PQ}}{\Delta_{PQ}} \right) \log \left( \frac{M_Q^2}{M_P^2} \right) - \frac{\lambda_{PQ}}{s} \log \left[ \frac{(s + \lambda_{PQ})^2 - \Delta_{PQ}^2}{(s - \lambda_{PQ})^2 - \Delta_{PQ}^2} \right] \right\},\end{aligned}\tag{A.1}$$

with

$$\Sigma_{PQ} \equiv M_P^2 + M_Q^2; \quad \Delta_{PQ} \equiv M_P^2 - M_Q^2; \quad \lambda_{PQ}^2 \equiv [s - (M_P + M_Q)^2] [s - (M_P - M_Q)^2].$$

From  $\bar{J}_{PQ}(s)$ , one defines the related quantities:

$$J_{PQ}^r(s) \equiv \bar{J}_{PQ}(s) - 2k_{PQ}(\mu); \quad K_{PQ}(s) \equiv \frac{\Delta_{PQ}}{2s} \bar{J}_{PQ}(s); \quad L_{PQ}(s) \equiv \frac{\Delta_{PQ}^2}{4s} \bar{J}_{PQ}(s); \tag{A.2}$$

and

$$M_{PQ}^r(s) \equiv \frac{1}{12s} (s - 2\Sigma_{PQ}) \bar{J}_{PQ}(s) + \frac{\Delta_{PQ}^2}{3s^2} [\bar{J}_{PQ}(s) - sJ_{PQ}'] - \frac{1}{6}k_{PQ}(\mu) + \frac{1}{288\pi^2}. \tag{A.3}$$

Here,

$$\begin{aligned}k_{PQ}(\mu) &\equiv \frac{1}{32\pi^2\Delta_{PQ}} [M_P^2 \log(M_P^2/\mu^2) - M_Q^2 \log(M_Q^2/\mu^2)], \\ J_{PQ}' &\equiv \frac{1}{32\pi^2} \left\{ \frac{\Sigma_{PQ}}{\Delta_{PQ}^2} + 2\frac{M_P^2 M_Q^2}{\Delta_{PQ}^3} \log \left( \frac{M_Q^2}{M_P^2} \right) \right\},\end{aligned}\tag{A.4}$$

and  $\mu$  denotes the renormalisation scale.

## B $\eta$ - $\eta'$ mixing

Let us consider the two-dimensional space of isoscalar pseudoscalar mesons. We collect the SU(3) octet and singlet fields in the doublet  $\eta_B^T \equiv (\eta_8, \eta_1)$ . The quadratic term in the Lagrangian takes the form

$$\mathcal{L} = \frac{1}{2} \partial_\mu \eta_B^T \mathcal{K} \partial^\mu \eta_B - \frac{1}{2} \eta_B^T \mathcal{M}^2 \eta_B, \quad (\text{B.1})$$

with

$$\mathcal{K} = \begin{pmatrix} 1 + \epsilon_8 & \delta \\ \delta & 1 + \epsilon_1 \end{pmatrix}, \quad \mathcal{M}^2 = \begin{pmatrix} M_8^2 & M_{18}^2 \\ M_{18}^2 & M_1^2 \end{pmatrix}. \quad (\text{B.2})$$

The coupling to the scalar resonances generates a  $\mathcal{K} \neq I_2$  kinetic matrix,

$$\epsilon_8 = \frac{8c_d c_m}{f^2 M_S^2} \overset{0}{M}_8^2, \quad \epsilon_1 = \frac{8c_d c_m}{f^2 M_S^2} \overset{0}{M}_1^2, \quad \delta = -\frac{2\sqrt{2}}{3} \frac{8c_d c_m}{f^2 M_S^2} \Delta_{K\pi}, \quad (\text{B.3})$$

and modifies the lowest-order values of the mass-matrix elements:

$$\begin{aligned} M_8^2 &= \overset{0}{M}_8^2 + \frac{8c_m^2}{f^2 M_S^2} \left( M_\pi^4 + \frac{8}{3} M_K^2 \Delta_{K\pi} \right), \\ M_1^2 &= M_0^2 + \overset{0}{M}_1^2 + \frac{8c_m^2}{f^2 M_S^2} \left( M_\pi^4 + \frac{4}{3} M_K^2 \Delta_{K\pi} \right), \\ M_{18}^2 &= -\frac{2\sqrt{2}}{3} \overset{0}{\Delta}_{K\pi} \left( 1 + \frac{8c_m^2}{f^2 M_S^2} 2M_K^2 \right). \end{aligned} \quad (\text{B.4})$$

Here,  $M_0^2$  denotes the  $U(1)_A$  anomaly contribution to the  $\eta_1$  mass,  $\overset{0}{M}_i^2$  ( $i = 1, 8$ ) the  $\mathcal{O}(p^2)$  contributions to the singlet and octet isoscalar masses,

$$\overset{0}{M}_8^2 = \frac{1}{3} \left( 4 \overset{0}{M}_K^2 - \overset{0}{M}_\pi^2 \right), \quad \overset{0}{M}_1^2 = \frac{1}{3} \left( 2 \overset{0}{M}_K^2 + \overset{0}{M}_\pi^2 \right), \quad (\text{B.5})$$

and  $\overset{0}{\Delta}_{K\pi} \equiv \overset{0}{M}_K^2 - \overset{0}{M}_\pi^2$ , with  $\overset{0}{M}_\pi^2$  and  $\overset{0}{M}_K^2$  the pion and kaon masses at  $\mathcal{O}(p^2)$  in the chiral expansion.

To first order in  $\epsilon_1$ ,  $\epsilon_8$  and  $\delta$ , the kinetic matrix  $\mathcal{K}$  can be diagonalised through the following field redefinition:

$$\eta_B = Z^{1/2} \cdot \hat{\eta} \equiv Z^{1/2} \cdot \begin{pmatrix} \hat{\eta}_8 \\ \hat{\eta}_1 \end{pmatrix}, \quad Z^{1/2 T} \cdot \mathcal{K} \cdot Z^{1/2} = I_2, \quad Z^{1/2} = \begin{pmatrix} 1 - \frac{\epsilon_8}{2} & -\frac{\delta}{2} \\ -\frac{\delta}{2} & 1 - \frac{\epsilon_1}{2} \end{pmatrix}. \quad (\text{B.6})$$



In the  $\hat{\eta}$  basis the mass matrix takes the form

$$\hat{\mathcal{M}} = Z^{1/2T} \cdot \mathcal{M} \cdot Z^{1/2}, \quad (\text{B.7})$$

where

$$\begin{aligned} \hat{M}_8^2 &= \hat{M}_8^2 + \frac{8c_m(c_m - c_d)}{f^2 M_S^2} \left( M_\pi^4 + \frac{8}{3} M_K^2 \Delta_{K\pi} \right), \\ \hat{M}_1^2 &= M_0^2 \left( 1 - \frac{8c_m c_d}{f^2 M_S^2} \hat{M}_1^2 \right) + \hat{M}_1^2 + \frac{8c_m(c_m - c_d)}{f^2 M_S^2} \left( M_\pi^4 + \frac{4}{3} M_K^2 \Delta_{K\pi} \right), \\ \hat{M}_{18}^2 &= -\frac{2\sqrt{2}}{3} \Delta_{K\pi} \left( 1 + \frac{8c_m(c_m - c_d)}{f^2 M_S^2} 2M_K^2 - \frac{4c_m c_d}{f^2 M_S^2} M_0^2 \right). \end{aligned} \quad (\text{B.8})$$

The physical mass eigenstates are obtained by diagonalising the matrix  $\hat{\mathcal{M}}$  with an orthogonal transformation,

$$\hat{\mathcal{M}} = \mathcal{R}^T \cdot \mathcal{M}_D \cdot \mathcal{R}, \quad \hat{\eta} = \mathcal{R}^T \cdot \eta_P \equiv \mathcal{R}^T \cdot \begin{pmatrix} \eta \\ \eta' \end{pmatrix}, \quad \mathcal{R} \equiv \begin{pmatrix} \cos \theta_P & -\sin \theta_P \\ \sin \theta_P & \cos \theta_P \end{pmatrix}. \quad (\text{B.9})$$

One gets the relations

$$M_{\eta'}^2 + M_\eta^2 = \hat{M}_1^2 + \hat{M}_8^2, \quad M_{\eta'}^2 - M_\eta^2 = \sqrt{(\hat{M}_1^2 - \hat{M}_8^2)^2 + 4\hat{M}_{18}^4}, \quad (\text{B.10})$$

and

$$\tan \theta_P = \frac{\hat{M}_8^2 - M_\eta^2}{\hat{M}_{18}^2} = \frac{M_{\eta'}^2 - \hat{M}_1^2}{\hat{M}_{18}^2} = \frac{\hat{M}_{18}^2}{M_{\eta'}^2 - \hat{M}_8^2} = \frac{\hat{M}_{18}^2}{\hat{M}_1^2 - M_\eta^2}. \quad (\text{B.11})$$

## C Inelastic channels

$$\begin{aligned}
T_{K\pi \rightarrow K\eta_1} = & \frac{1}{\sqrt{2}f_K^2} \left\{ \frac{2M_K^2 + M_\pi^2}{3} + \frac{2c_m c_d \Delta_{K\pi}}{3f^2 M_S^2} (3t - p_\eta^2 + M_\pi^2) - \frac{8c_m^2 \Delta_{K\pi}^2}{3f^2 M_S^2} \right. \\
& + \frac{2}{f^2} \left[ \frac{c_d s + (c_m - c_d) \Sigma_{K\pi}}{M_{K_0^*}^2 - s} [c_d (s - p_\eta^2 - M_K^2) + 2c_m M_K^2] \right. \\
& + \frac{c_d u + (c_m - c_d) \Sigma_{K\pi}}{M_{K_0^*}^2 - u} [c_d (u - p_\eta^2 - M_K^2) + 2c_m M_K^2] \\
& \left. \left. + \frac{c_d t + 2(c_m - c_d) M_K^2}{M_{a_0}^2 - t} [c_d (t - p_\eta^2 - M_\pi^2) + 2c_m M_\pi^2] \right] \right\}, \quad (C.1)
\end{aligned}$$

$$\begin{aligned}
T_{K\pi \rightarrow K\eta_8} = & \frac{1}{4f_K^2} \left\{ 3t - p_\eta^2 - \frac{8}{3} M_K^2 - \frac{1}{3} M_\pi^2 + \frac{4c_m c_d \Delta_{K\pi}}{3f^2 M_S^2} (3t + 2p_\eta^2 - 2M_\pi^2) - \frac{4c_m^2 \Delta_{K\pi}^2}{3f^2 M_S^2} \right. \\
& + \frac{2}{f^2} \left[ \frac{c_d s + (c_m - c_d) \Sigma_{K\pi}}{M_{K_0^*}^2 - s} [c_m (3M_\pi^2 - 5M_K^2) - c_d (s - p_\eta^2 - M_K^2)] \right. \\
& + \frac{c_d u + (c_m - c_d) \Sigma_{K\pi}}{M_{K_0^*}^2 - u} [c_m (3M_\pi^2 - 5M_K^2) - c_d (u - p_\eta^2 - M_K^2)] \\
& + 2 \frac{c_d t + 2(c_m - c_d) M_K^2}{M_{a_0}^2 - t} [2c_m M_\pi^2 + c_d (t - p_\eta^2 - M_\pi^2)] \\
& \left. + \frac{3G_V^2}{f^2} \left[ \frac{s(t - u) - (p_\eta^2 - M_K^2) \Delta_{K\pi}}{M_{K^*}^2 - s} + \frac{u(t - s) - (p_\eta^2 - M_K^2) \Delta_{K\pi}}{M_{K^*}^2 - u} \right] \right\}, \quad (C.2)
\end{aligned}$$

$$\begin{aligned}
T_{K\eta_1 \rightarrow K\eta_1} = & \frac{4}{3f_K^2} \left\{ \frac{1}{2} M_K^2 - \frac{4c_m c_d \Delta_{K\pi}}{3f^2 M_S^2} \right. \\
& + \frac{1}{f^2} \left[ \frac{1}{M_{K_0^*}^2 - s} [c_d (s - k_\eta^2 - M_K^2) + 2c_m M_K^2] [c_d (s - k_\eta'^2 - M_K^2) + 2c_m M_K^2] \right. \\
& + \frac{1}{M_{K_0^*}^2 - u} [c_d (u - k_\eta^2 - M_K^2) + 2c_m M_K^2] [c_d (u - k_\eta'^2 - M_K^2) + 2c_m M_K^2] \\
& + \frac{1}{M_{S_1}^2 - t} [c_d t + 2(c_m - c_d) M_K^2] [c_d (t - k_\eta^2 - k_\eta'^2) + \frac{2}{3} c_m (2M_K^2 + M_\pi^2)] \\
& \left. \left. + \frac{2}{3} \frac{c_m \Delta_{K\pi}}{M_S^2 - t} [c_d t + 2(c_m - c_d) M_K^2] \right] \right\}, \quad (C.3)
\end{aligned}$$

$$\begin{aligned}
T_{K\eta_1 \rightarrow K\eta_8} = & -\frac{\sqrt{2}}{3f_K^2} \left\{ M_K^2 - \frac{1}{2}M_\pi^2 - \frac{c_m c_d \Delta_{K\pi}}{3f^2 M_S^2} (9t - 3k_\eta^2 + 3k_\eta'^2 + 16\Delta_{K\pi}) + \frac{4c_m^2 \Delta_{K\pi}^2}{f^2 M_S^2} \right. \\
& + \frac{1}{f^2} \left[ \frac{1}{M_{K_0^*}^2 - s} \left[ c_d (s - k_\eta^2 - M_K^2) + 2c_m M_K^2 \right] \left[ c_d (s - k_\eta'^2 - M_K^2) + c_m (5M_K^2 - 3M_\pi^2) \right] \right. \\
& + \frac{1}{M_{K_0^*}^2 - u} \left[ c_d (u - k_\eta^2 - M_K^2) + 2c_m M_K^2 \right] \left[ c_d (u - k_\eta'^2 - M_K^2) + c_m (5M_K^2 - 3M_\pi^2) \right] \\
& + \frac{1}{M_S^2 - t} \left[ c_d t + 2(c_m - c_d)M_K^2 \right] \left[ c_d (t - k_\eta^2 - k_\eta'^2) + \frac{2}{3} c_m (4M_K^2 - M_\pi^2) \right] \\
& \left. \left. + \frac{16}{3} \frac{c_m \Delta_{K\pi}}{M_{S_1}^2 - t} \left[ c_d t + 2(c_m - c_d)M_K^2 \right] \right] \right\}, \quad (C.4)
\end{aligned}$$

$$\begin{aligned}
T_{K\eta_8 \rightarrow K\eta_8} = & \frac{1}{6f_K^2} \left\{ \frac{1}{2} (9t - 3k_\eta^2 - 3k_\eta'^2 - 2M_\pi^2) - \frac{2c_m c_d \Delta_{K\pi}}{3f^2 M_S^2} (9t + 32\Delta_{K\pi}) + \frac{14c_m^2 \Delta_{K\pi}^2}{f^2 M_S^2} \right. \\
& + \frac{1}{f^2} \left[ \frac{1}{M_{K_0^*}^2 - s} \left[ c_d (s - k_\eta^2 - M_K^2) + c_m (5M_K^2 - 3M_\pi^2) \right] \left[ c_d (s - k_\eta'^2 - M_K^2) + c_m (5M_K^2 - 3M_\pi^2) \right] \right. \\
& + \frac{1}{M_{K_0^*}^2 - u} \left[ c_d (u - k_\eta^2 - M_K^2) + c_m (5M_K^2 - 3M_\pi^2) \right] \left[ c_d (u - k_\eta'^2 - M_K^2) + c_m (5M_K^2 - 3M_\pi^2) \right] \\
& + \frac{2}{M_S^2 - t} \left[ c_d t + 2(c_m - c_d)M_K^2 \right] \left[ c_d (t - k_\eta^2 - k_\eta'^2) + \frac{2}{3} c_m (8M_K^2 - 5M_\pi^2) \right] \\
& + \frac{8}{M_{S_1}^2 - t} \left[ c_d t + 2(c_m - c_d)M_K^2 \right] \left[ c_d (t - k_\eta^2 - k_\eta'^2) + \frac{2}{3} c_m (4M_K^2 - M_\pi^2) \right] \\
& \left. \left. + \frac{9G_V^2}{2f^2} \left[ \frac{s(t-u) + (k_\eta^2 - M_K^2)(k_\eta'^2 - M_K^2)}{M_{K^*}^2 - s} + \frac{u(t-s) + (k_\eta^2 - M_K^2)(k_\eta'^2 - M_K^2)}{M_{K^*}^2 - u} \right] \right] \right\}. \quad (C.5)
\end{aligned}$$

Several remarks concerning the above expressions are in order.  $p_\eta$ ,  $k_\eta$  and  $k_\eta'$  are momenta of the  $\eta_i$ 's. In eqs. (C.3) to (C.5),  $k_\eta$  refers to the initial state  $\eta_i$  and  $k_\eta'$  to the final state  $\eta_j$ . For example in the calculation of the amplitude  $T_{K\eta \rightarrow K\eta'}$ , we have  $k_\eta^2 = M_\eta^2$  and  $k_\eta'^2 = M_{\eta'}^2$ .

## D Input parameters

For the convenience of the reader, in this appendix we collect the values of all constant input parameters used in our numerical analysis:

$$M_\pi = 138.0 \text{ MeV}, \quad M_K = 495.7 \text{ MeV},$$

$$M_\eta = 547.3 \text{ MeV}, \quad M_{\eta'} = 957.8 \text{ MeV},$$

$$f_\pi = 92.4 \text{ MeV}, \quad f_K = 112.7 \text{ MeV},$$

$$M_\rho = 770.0 \text{ MeV}, \quad M_{K^*} = 896.1 \text{ MeV},$$

$$M_{V'} = 1440 \text{ MeV}, \quad M_{V''} = 1710 \text{ MeV},$$

$$G_V = f_\pi/\sqrt{2} = 65.3 \text{ MeV},$$

$$G_{V'} = 12 \text{ MeV}, \quad G_{V''} = 23 \text{ MeV},$$

$$M_S = M_{S_1}, \quad M_{S'} = M_{S'_1},$$

$$\sin \theta = -1/3 \approx 20^\circ.$$

## References

- [1] S. WEINBERG, *Physica* **A96** (1979) 327.
- [2] J. GASSER and H. LEUTWYLER, *Ann. Phys.* **158** (1984) 142.
- [3] J. GASSER and H. LEUTWYLER, *Nucl. Phys.* **B250** (1985) 465.
- [4] U.-G. MEISSNER, *Rep. Prog. Phys.* **56** (1993) 903.
- [5] G. ECKER, *Prog. Part. Nucl. Phys.* **35** (1995) 1.
- [6] A. PICH, *Rep. Prog. Phys.* **58** (1995) 563.
- [7] V. BERNARD, N. KAISER, and U.-G. MEISSNER, *Int. J. Mod. Phys.* **E4** (1995) 193.
- [8] G. ECKER, J. GASSER, A. PICH, and E. DE RAFAEL, *Nucl. Phys.* **B321** (1989) 311.
- [9] G. ECKER, J. GASSER, H. LEUTWYLER, A. PICH, and E. DE RAFAEL, *Phys. Lett.* **B223** (1989) 425.
- [10] G. 'T HOOFT, *Nucl. Phys.* **B72** (1974) 461.
- [11] E. WITTEN, *Nucl. Phys.* **B160** (1979) 57.
- [12] S. PERIS, M. PERROTET, and E. DE RAFAEL, *JHEP* **5** (1998) 11.
- [13] T. N. TRUONG, *Phys. Rev. Lett.* **61** (1988) 2526.
- [14] A. DOBADO, M. J. HERRERO, and T. N. TRUONG, *Phys. Lett.* **B235** (1990) 134.
- [15] N. KAISER, P. D. SIEGEL, and W. WEISE, *Nucl. Phys.* **A594** (1995) 325.
- [16] J. A. OLLER and E. OSET, *Nucl. Phys.* **A620** (1997) 438, Erratum *Nucl. Phys.* **A652** (1999) 407.
- [17] F. GUERRERO and A. PICH, *Phys. Lett.* **B412** (1997) 382.
- [18] F. GUERRERO, *Phys. Rev.* **D57** (1998) 4136.
- [19] J. A. OLLER, E. OSET, and J. R. PELÁEZ, *Phys. Rev. Lett.* **80** (1998) 3452, *Phys. Rev.* **D59** (1999) 074001.
- [20] J. A. OLLER and E. OSET, *Phys. Rev.* **D60** (1999) 074023.

- [21] J. A. OLLER, E. OSET, and A. RAMOS, hep-ph/0002193, to appear in *Prog. Part. Nucl. Phys.* **45** (2000) .
- [22] S. NARISON, N. PAVER, E. DE RAFAEL, and D. TRELEANI, *Nucl. Phys.* **B212** (1983) 365.
- [23] M. JAMIN and M. MÜNZ, *Z. Phys.* **C60** (1993) 569.
- [24] K. G. CHETYRKIN, C. A. DOMINGUEZ, D. PIRJOL, and K. SCHILCHER, *Phys. Rev.* **D51** (1995) 5090.
- [25] P. COLANGELO, F. DE FAZIO, G. NARDULLI, and N. PAVER, *Phys. Lett.* **B408** (1997) 340.
- [26] M. JAMIN, *Nucl. Phys. B (Proc. Suppl.)* **64** (1998) 250, Proc. of *QCD 97*, Montpellier, July 1997.
- [27] T. BHATTACHARYA, R. GUPTA, and K. MALTMAN, *Phys. Rev.* **D57** (1998) 5455.
- [28] M. JAMIN, J. A. OLLER, and A. PICH, *in preparation* .
- [29] V. BERNARD, N. KAISER, and U.-G. MEISSNER, *Nucl. Phys.* **B357** (1991) 129.
- [30] V. BERNARD, N. KAISER, and U.-G. MEISSNER, *Nucl. Phys.* **B364** (1991) 283.
- [31] C. B. LANG, *Fort. d. Phys.* **26** (1978) 509.
- [32] S. WEINBERG, *Phys. Rev. Lett.* **17** (1966) 616.
- [33] A. ROESSL, *Nucl. Phys.* **B555** (1999) 507.
- [34] I. S. GRADSHTEYN and I. M. RYZHIK, *Tables of integrals, series, and products*, Academic Press, 1980.
- [35] G. F. CHEW and S. MANDELSTAM, *Phys. Rev.* **119** (1960) 467.
- [36] J. A. OLLER, *Phys. Lett.* **B477** (2000) 187.
- [37] U.-G. MEISSNER and J. A. OLLER, nucl-th/9912026, *Nucl. Phys.* **A673** (2000) 311.
- [38] P. ESTABROOKS ET AL., *Nucl. Phys.* **B133** (1978) 490.
- [39] D. ASTON ET AL., *Nucl. Phys.* **B296** (1988) 493.

- [40] N. AWAJI, *Ph.D. thesis*, Nagoya University, 1986, (unpublished).
- [41] B. JONGEJANS ET AL., *Nucl. Phys.* **B67** (1973) 381.
- [42] D. LINGLIN ET AL., *Nucl. Phys.* **B57** (1973) 64.
- [43] A. M. BAKKER ET AL., *Nucl. Phys.* **B24** (1970) 211.
- [44] Y. CHO ET AL., *Phys. Lett.* **32B** (1970) 409.
- [45] C. CASO ET AL., *Eur. Phys. J. C* **3** (1998) 1.
- [46] G. AMORÓS, J. BIJNENS, and P. TALAVERA, *Phys. Lett.* **B480** (2000) 71.
- [47] G. AMORÓS, J. BIJNENS, and P. TALAVERA, *University of Lund preprint*, **hep-ph/0003258** (2000).
- [48] J. WEINSTEIN and N. ISGUR, *Phys. Rev Lett.* **48** (1982) 659.
- [49] G. JANSEN, B. C. PEARCE, K. HOLINDE, and J. SPETH, *Phys. Rev.* **D52** (1995) 2690.
- [50] C. AMSLER and F. E. CLOSE, *Phys. Rev.* **D53** (1996) 295.
- [51] V. ELIAS, A. H. FARIBORZ, F. SHI, and T. G. STEELE, *Nucl. Phys.* **A633** (1998) 279.
- [52] D. MORGAN, *Phys. Lett.* **51B** (1974) 71.
- [53] N. N. ACHASOV and G. N. SHESTAKOV, *Phys. Rev.* **D49** (1991) 5779.
- [54] N. A. TÖRNQVIST, *Z. Phys.* **C68** (1995) 647.
- [55] F. JAMES, *Minuit Reference Manual* **D506** (1994).
- [56] A. DOBADO and J. R. PELÁEZ, *Phys. Rev.* **D47** (1993) 4883.
- [57] C. LANG, *Nucl. Phys.* **B93** (1975) 415.
- [58] C. B. LANG and W. POROD, *Phys. Rev.* **D21** (1980) 1295.
- [59] P. HERRERA-SIKLÓDY ET AL., *Nucl. Phys.* **B497** (1997) 345.
- [60] P. HERRERA-SIKLÓDY ET AL., *Phys. Lett.* **B419** (1998) 326.

- [61] H. LEUTWYLER, *Phys. Lett.* **B374** (1996) 163.
- [62] E. BARRELET, *Nuovo Cim.* **8A** (1972) 331.
- [63] C. B. LANG and I. S. STEFANESCU, *Phys. Lett.* **B79** (1978) 479.
- [64] R. L. JAFFE, *Phys. Rev.* **D15** (1977) 267, 281.
- [65] M. D. SCADRON, *Phys. Rev.* **D26** (1982) 239.
- [66] E. VAN BEVEREN ET AL., *Z. Phys.* **C30** (1986) 615.
- [67] S. ISHIDA ET AL., *Prog. Theor. Phys.* **98** (1997) 621.
- [68] R. DELBOURGO and M. D. SCADRON, *Int. J. Mod. Phys.* **A13** (1998) 657.
- [69] D. BLACK, A. H. FARIBORZ, F. SANNINO, and J. SCHECHTER, *Phys. Rev.* **D58** (1998) 054012.
- [70] A. V. ANISOVITCH and A. V. SARANTSEV, *Phys. Lett.* **B413** (1997) 137.
- [71] S. N. CHERRY and M. R. PENNINGTON, **hep-ph/0005208** (2000).